Suitability of ground-based SfM-MVS for monitoring glacial and periglacial processes

~~Analysis of glacial and periglacial processes using structure from motion~~

L. Piermattei[1], L. Carturan[1], F. de Blasi[1], P. Tarolli[1], G. Dalla Fontana[1], A. Vettore[2] and N. Pfeifer[3].

[1]Department of Land, Environment, Agriculture and Forestry, University of Padova, Italy

[2]Interdepartment Research Center of Geomatics, University of Padova, Italy

[3]Department of Geodesy and Geoinformation, TU Wien, Austria

Correspondence to: L. Piermattei (livia.piermattei@studenti.unipd.it)

Abstract

P~~Close-range p~~hoto-based surface reconstruction from the ground is rapidly emerging as an alternative survey technique to LiDAR (light detection and ranging), ~~which today represents the main survey technique~~ in many fields of geoscience, fostered by the recent ~~. The recent evolution of photogrammetry, incorporating~~development of computer vision algorithms such as Structure from Motion (SfM) and dense image matching such as Multi-View Stereo (MVS)., ~~allows the reconstruction of dense 3-D point clouds for the photographed object from a sequence of overlapping images taken with a digital consumer camera.~~ The objective of ~~our~~ this work was to test the ~~accuracy of~~suitability of ~~-~~the ground-based SfM-MVS approach in calculating the geodetic mass balance of a 2.1 km^2 glacier and for the detection of the surface displacement rate of a neighbouring active rock glacier located ~~in the Ortles-Cevedale Group,~~ in the Eastern Italian Alps. ~~In addition, we investigated the feasibility of using the image-based approach for the detection of the surface displacement rate of a neighbouring active rock glacier.~~ The ~~terrestrial surveys were~~ photos were acquired in 2013 and 2014 using a digital consumer-grade camera, organizing single-day field surveys.~~planned to be quick with a low budget and conducted in a safe and easy way in a single day.~~ Airborne laser scanning (ALS) data were used as benchmarks to estimate the accuracy of the photogrammetric digital elevation models (DEMs) and the reliability of the method. ~~in this specific applications.~~ The ~~results were encouraging because the~~ SfM-MVS approach enable~~s~~d the reconstruction of high-quality DEMs, which provided estimates of glacial

and periglacial processes similar to those achievable by ALS. ~~The glacial and periglacial analyses were performed using both range and image-based surveying techniques, and the results were then compared.~~ In stable bedrock areas outside the glacier, the ~~The accuracy of the photogrammetric DEMs, evaluated as the~~ mean and the standard deviation of the elevation difference ~~in a stable area~~ between the SfM-MVS DEM and the ~~reference~~ ALS DEM~~,~~ was -0.42 m ± 1.72 m and 0.03 m ± 0.74 m ~~for the~~in 2013 and 2014 ~~surveys~~, respectively. In the rock glacier area, the elevation difference was~~The SfM-MVS DEM accuracy of the reconstructed rock glacier surface acquired in 2014 was estimated to be~~ 0.02 m ± 0.17 m. The use of natural targets as ground control points, the occurrence of shadowed and low-contrast areas, and in particular the sub-optimal camera network geometry imposed by the morphology of the study area were the main factors affecting the accuracy of photogrammetric DEMs.

~~Different resolutions and accuracies were obtained for the glacier and the rock glacier, given the different survey geometries, surface characteristics and areal extents. The analysis of the SfM-MVS DEM quality allowed us to highlight the limitations of the adopted expeditious method in the studied alpine terrain and the potential of this method in the multitemporal study of glacial and periglacial areas.~~

1. Introduction

Knowledge of changes in the extent, mass and surface velocity of glaciers and rock glaciers contributes to better understanding the dynamic processes occurring in cold high-mountain environments and serves as an important contribution to climate monitoring (Kääb et al., 2003).

Numerous techniques exist for monitoring and quantifying these changes and include both field and remote sensing methods (Immerzeel et al., 2014). Fieldwork generally yields high-quality data but with a small spatial extent, given the remoteness and low accessibility of mountain areas at high elevations (Roer et al., 2007). Therefore, using remotely sensed datasets for at least two different points in time has become an important tool for monitoring high-mountain terrain dynamics (Kääb, 2002). Multitemporal Digital ~~Terrain~~ Elevation Models (DEMs) based on remote sensing data are the most commonly used products for such investigations (Kääb, 2005; Tseng et al., 2015).

~~Among the many remote sensing techniques, aerial photogrammetry is the oldest method, and it has a long history of application in the study of glaciers (Welch and Howarth, 1968; Kääb and Funk, 1999; Schenk, 1999; Baltsavias et al., 2001; Kääb 2005; Haug et al., 2009; Bühler et al., 2014; Müller et al., 2014) and the monitoring of rock glaciers via repeated stereo images (Kääb et al., 1997; Kaufmann, 1998; Kääb, 2003; Fischer, 2011). Terrestrial (ground-based or close-range) photogrammetry was one of the first measurement techniques used to map high mountain terrain and for reliably measuring the flow velocity of a rock glacier (Kaufmann and Ladstädter 2007; Kaufmann, 2012) until it was replaced by aerial and spaceborne platforms (Pellikka and Rees, 2009).~~

~~Over the last decade, the photogrammetric technique has widely been replaced by LiDAR (light detection and ranging) technology, which has progressively become the primary survey technique in geomorphology (Tarolli, 2014). Aerial laser scanning (ALS) is reported to be a very accurate method for DEMs generation in alpine terrain (Bülher and Graf, 2013, Aguilar and Mills, 2008; Höfle and Rutzinger, 2011), snow covered areas (Höfle et al., 2007; Deems et al., 2013) and glacial environments (Geist Stotter, 2007; Kodde et al., 2007; Abermann et al., 2010; Knoll and Kerschner, 2010; Carturan et al., 2013; Colucci et al., 2014; Joerg and Zemp, 2014). However, aerial LiDAR surveys are still expensive and terrestrial LiDAR surveys involve expensive and logistically demanding equipment.~~

Among the available remote sensing techniques, the~~The~~ close-range photogrammetry saw a rapid development thanks to the recent evolution of digital photogrammetry, based on computer vision algorithms. This technique is~~, has led to a rapid revival of close-range photogrammetry~~ becoming ~~as~~ the major alternative to traditional surveying techniques and LiDAR (light detection and ranging) technolog~~y~~ies, due to its lower cost, high portability, and easy and rapid surveying in the field.

The photogrammetric approach known as Structure from Motion (SfM) allows ~~to~~ ~~obtains~~obtaining 3D information ~~on~~ of the photographed object from a sequence of overlapping images taken with a ~~consumer-grade~~ digital camera. ~~The ability to obtain 3D models with accuracies and resolutions comparable to those of LiDAR has created new opportunities, especially in geoscience applications in remote areas (James and Robson, 2012; Bemis et al., 2014; Micheletti et al., 2014; Prosdocimi et~~

~~al., 2015; Stumpf et al., 2015). An overview of the SfM applications and accuracy assessments is given by Clapuyt et al. (2015).~~

A limited number of ~~studies~~ applications of ~~close-range~~SfM ~~-~~photogrammetry in glacial and periglacial environments exists, and they principally involve the use of Unmanned Aerial Vehicles (UAVs) for image acquisition (Solbø S. and Storvold R. 2013; Whitehead et al., 2013; Immerzeel et al., 2014, Tonkin et al., 2014; Gauthier et al., 2014; Bühler et al., 2014; Dall'Asta et al., 2015~~a~~; Ryan et al., 2015) rather than ground-based surveys (Gómez-Gutiérrez et al., 2014; 2015; Kääb et al., 2014; Piermattei et al., 2015). ~~Kääb et al. (2014) tested the time-lapse SfM approach in the measurement of vertical and horizontal changes in periglacial patterned grounds.~~

The objective of our work was to assess the ~~potential and the limits~~suitability of the ground-based SfM approach ~~in~~ ifor monitoring glacial and periglacial processes in a high-altitude area of the Ortles-Cevedale Group (Eastern Italian Alps). In particular, ~~we used the~~ this approach was used to calculate the geodetic annual mass balance of a 2.1 ~~-~~km^2 glacier and to detect the surface displacement of a neighbouring 0.06 ~~-~~ km^2 rock glacier. The photogrammetric surveys were intentionally planned to be as quick and cost-effective as possible, and easily replicable in the future. Therefore, a consumer-grade camera was adopted to find an appropriate balance between the affordability and accessibility of the system (i.e. cost and ease of use) and the quality of the resulting topographic data (accuracy and density). The accuracy of the photogrammetric DEMs was estimated using ALS-based DEMs acquired during the same periods. The main factors affecting the accuracy of the photogrammetric DEMs were investigated, and the significance of the biases in the quantification of glacial and periglacial processes was discussed.

2. Geographical setting and ~~C~~case studies

The La Mare Glacier and the neighbouring AVDM3 Rock Glacier are located in the south-eastern part of the Ortles-Cevedale massif (Eastern Italian Alps), the largest glaciated mountain group of the Italian Alps (Fig. 1).

The La Mare Glacier (World Glacier Inventory code I4L00102517; WGMS 1989) is a 3.55 km^2 valley glacier currently composed of two ice bodies, which have different morphologies and tend to separate (Carturan et al., 2014). In this work, ~~we focused~~

the focus was on the southern ice body, which feeds the main tongue. This 2.1 km^2 ice body primarily faces north-east, and its surface is rather flat, with the exception of the small remnant of its valley tongue. The elevation ranges from 2660 to 3590 m a.s.l. Mass balance investigations using the direct glaciological method were started on La Mare Glacier in 2003 and detected an average annual mass balance of -0.76 m w.e. y^{-1} during the period from 2003 to 2014 (Carturan, ~~2015~~2016). The mass balance was close to zero in 2013 (-0.06 m w.e.) and was positive for the first time since the beginning of measurements in 2014 (+0.83 m w.e.).

The AVDM3 Rock Glacier (Carturan et al., 2015) is an intact, tongue-shaped rock glacier characterized by the presence of two lobes. The 0.058 km^2 wide Rock Glacier (maximum length of 390 m; maximum width of 240 m) faces south-east and is located at elevations of between 2943 and 3085 m a.s.l. The average slope of the Rock Glacier is 26°, and the slope of the advancing front is 36°. The activity status of the AVDM3 Rock Glacier was assessed via repeated geomorphological field surveys between 2007 and 2014. These surveys revealed the advance of the front of the southern lobe (Carturan, 2010). The general morphology and the elevation of the front also suggest that this rock glacier is active (Seppi et al., 2012), and its permafrost content is further corroborated by spring temperature measurements (Carturan et al., 2015). Moreover, Bertone (2014) provided the first quantification of the surface displacement rates of this rock glacier for 2003 to 2013 using ALS data.

3. Methods

~~In this section, we briefly describe the ALS data that were used to i) select the ground control points (GCPs) required to scale and georeference the SfM 3D models, ii) co-register the point clouds before producing the DEMs, and iii) validate the photogrammetric results. Then, we describe how the photogrammetric surveys were performed and processed to produce the dense point clouds and DEMs of the La Mare Glacier and AVDM3 Rock Glacier~~

3.1 The ALS data

ALS flights of the study area were available for 17 September 2003, 22 September 2013, and 24 September 2014. The technical specifications of the three ALS surveys are reported in Table 1. To avoid errors due to global shifts or rotations between the individual DEMs, ~~we automatically co-registered~~ the ALS point clouds were automatically co-registered using a version of the ICP algorithm (Chen and Medioni, 1991; Besl and McKay, 1992) tailored to topographic point clouds (Glira et al., 2015). The LiDAR point cloud acquired in 2013 was treated as a reference only for stable areas outside the glaciers, rock glaciers, snow patches, and geomorphologically active areas (e.g., landslides, river beds, and debris flows). The 2003 and 2014 LiDAR point clouds were iteratively fitted to the reference point cloud by applying an affine transformation. The ICP registration of the point clouds produced z-direction residual values of 0.08 m and 0.11 m for the 2014 and 2003 LiDAR point clouds, respectively. These accuracies can be assumed to be sufficient for calculating the annual elevation changes of the glacier and the decadal displacement rate on the rock glacier.

The co-registered point clouds were then converted to DEMs using Natural Neighbours interpolations. A pixel size of 1 x 1 m was produced for the La Mare Glacier, whereas a pixel size of 0.5 x 0.5 m was used for the rock glacier, based on the LiDAR point cloud density (Fig. 2). To evaluate the relative ALS DEM accuracies after the co-registration, the elevation difference errors of the DEMs were calculated for the stable areas. The standard deviation from the 2013 ALS DEM was 0.19 m and 0.21 m for the 2014 and 2003 DEM comparisons, respectively.

3.2 The photogrammetric workflow

3.2.1 Field surveys

The terrestrial photogrammetric surveys of the La Mare Glacier were conducted on 4 September 2013 and 27 September 2014, that is, close to the end of the mass balance year and of ALS flights. The timing of the surveys enabled the calculation of the annual mass balance of the glacier and ~~the ability~~ to compare the results with the ALS-based results. On both days, the sky was clear, with almost no cloud cover.

To guarantee a safe and easily repeatable survey of the glacier, ~~we avoided directly accessing its surface, instead performing~~ the direct access to its surface was avoided and ~~by performing~~ the survey was performed from a rocky ridge on the north side of the glacier (Fig. ~~4~~5). The elevation of the survey ranged from 3100 to 3300 m in 2013 and from 2600 to 3300 m in 2014. The distance from the glacier surface to the camera positions dictated by the topography ranged between 300 and 2900 m. To cover the entire glacier surface from these positions, the acquired images were panoramic, which involved taking a series of photographs rotating the camera from each individual camera position. In 2013, seven camera positions were used, and 37 photographs were taken with the camera attached to a small tripod to avoid camera shake. In 2014, the number of camera positions was increased to 21, and 177 photos were taken freehand (Fig. 3).

Both surveys were performed using a SLR Canon EOS 600D. The camera was equipped with a 25-70 mm zoom lens, which was set to a focal length of 25 mm in 2013 and 35 mm in 2014.

The terrestrial photogrammetric survey of the AVDM3 Rock Glacier was performed on 27 September 2014. In this survey, 198 images were acquired freehand while walking around and on top of the rock glacier. The survey camera was a CANON EOS 5D full frame SLR camera equipped with a fixed-focal lens of 28 mm. The photographs were acquired and saved in RAW format in both surveys.

3.2.2 Data processing

The latest evolution of photogrammetry is characterized by the combination of the principles of photogrammetry, such as bundle adjustment, and automatic computer vision algorithms, such as feature extraction and feature matching. This photogrammetric approach, called Structure from Motion (SfM), can automatically derive the 3D position of an object in images taken in sequence calculating the camera parameters (intrinsic and extrinsic) (Hartley and Zissermann, 2004). Dense image matching algorithms are then used to reconstruct the 3D model of the object as a dense point cloud. Multiple photogrammetric packages implementing SfM and Multi-View Stereo (MVS) algorithms for dense image matching exist, and in this work, ~~we used~~ the software PhotoScan Pro (AgiSoft LLC. 2010a) was used. Henceforth,

we refer to the photogrammetric surveys and results are referred to using the acronym SfM-MVS.

The photo-based reconstruction workflow is summarized in Fig. 4. The key components of the workflow are 1) acquisition and photograph editing, 2) GCPs identification, image feature detection, matching and 3D scene reproduction (the SfM-MVS steps), 3) point cloud processing, (filtering, subsampling and ICP) and 4) DEM reconstruction.

To overcome the significant variability in brightness during the surveys, the RAW images have been edited to adjust the exposure and contrast in order to retrieve information from the overexposed (e.g., snow-covered) areas and underexposed (e.g., shadowed) areas. These editing steps had a positive impact on the number of image features extracted. The edited images were saved in TIFF format and loaded in PhotoScan where non-stationary objects (i.e., clouds and shadows), the sky, and features lying in the distant background have been masked.

The camera calibration parameters were calculated using artificial targets prior to the processing of the photogrammetric surveys (pre-calibrated camera). The intrinsic parameters were kept constant during the entire SfM processing given the limits of the camera network geometry and the homogeneous texture of the surveyed terrain. As additional constraint, the GCPs were included into the SfM process to avoid instability in the bundle adjustment solution (Verhoeven et al., 2015). The GCPs were selected as natural features in stable area outside the glacier and rock glacier, and their coordinates were extracted from the 2013 ALS hillshaded DEM. After the SfM step, the geo-referenced dense point cloud was reconstructed by the MVS algorithm, using the 'mild' smoothing filter to preserve as much spatial information as possible (AgiSoft LLC., 2010b).

To reduce the noise and outliers generated during the dense matching reconstruction (Bradley et al., 2008; Nilosek et al., 2012), an initial filtering was performed in PhotoScan to manually remove the outliers. Further denoising was applied to the dense point clouds exported from PhotoScan, using a specific tool to treat the point clouds. To obtain a uniform spatial distribution of the points, the photogrammetric point clouds (much denser than the ALS point clouds), were down-sampled to 20 cm for the glacier and 10 cm for the rock glacier. Following the same procedure used for the ALS data, the ICP algorithm (OpalsICP, TU ViennaWien) was applied to co-register the point clouds in the stable area outside the glacier and rock glacier, using

the 2013 ALS point cloud as a reference. The co-registered point clouds were then converted to DEMs, using the Natural Neighbours interpolation and the pixel sizes of the ALS DEMs (i.e., 1 x 1 m for the glacier and 0.5 x 0.5 m for the rock glacier). The data acquisition settings and processing results of the photogrammetric surveys are summarized in Table 2.

3.3 Analyses

The accuracy of the photogrammetric DEMs was assessed ~~to calculate~~calculating the mean, the mean of the absolute values and the standard deviation (σ) of the elevation differences (DEM of Difference, DoD) between SfM-MVS DEMs and ALS DEMs, using the latter as a reference dataset. For both surveyed areas, the primary factors controlling the quality of the photogrammetric results~~DEMs~~ (i.e., camera–object distance, slope and angle of incidence, camera network geometry, surface texture and shadows) were evaluated in terms of DEM accuracy and spatial resolution. The obtained results were compared to ~~analysis of~~ the theoretical ~~error propagation~~behaviour of the error as a function of the depth (σ_d) ~~direction (camera-object distance), was~~ calculated using the following formulation:

$$\sigma_d = m_B \cdot \frac{D}{B} \cdot \sigma_i, \quad (1)$$

where m_B represents the image scale (*D / focal length*); *D* is the depth (camera-object distance); B is the baseline and σ_i is the measured accuracy in the image space.

After the accuracy assessments, we investigated the suitability of using the terrestrial photogrammetric surveys to calculate the annual mass balance of the glacier and the elevation change and ~~the~~ surface displacement rates of the rock glacier, comparing the results with those obtained from ALS surveys. The mass balance and elevation changes were calculated differencing multitemporal DEMs.

The geodetic mass balance was calculated from the total volume change ΔV (m^3) between two survey dates~~: using the following relation~~

$$V = \overline{\Delta z} \cdot A \quad (2)$$

where $\overline{\Delta z}$ is the average elevation change between two DEMs over the area *A* of the glacier. The area-averaged net geodetic mass balance in metres of water equivalent per year (m w.e. y^{-1}) was calculated as:

$$\dot{M} = \frac{\Delta V \cdot \rho}{A} \quad (3)$$

where ρ is the mean density. The area A of the glacier between the two surveys did not change. The mean density was obtained by a fractional area-weighted mean, assigning 900 kg/m^3 for the ablation area (Huss, 2013) and 530 kg/m^3 for the accumulation area, as directly measured in a snowpit. The resulting weighted mean density was 600 kg/m^3. In the mass balance calculations, both raw $\overline{\Delta z}$ values and corrected $\overline{\Delta z}$ values were used to account for the mean errors in the stable areas outside the glacier, as reported in Table 3. Other processes ~~–~~like ice fluxes~~,~~ ~~and~~ varying snow density ~~or~~and re-freezing of melt water were assumed to be negligible for the ~~not taken into account to estimate~~calculation of the annual geodetic mass balance.

The horizontal surface displacements rates of the AVDM3 rock glacier were estimated by ~~means of manual detection of features on the hillshaded DEMs.~~a manual measurement of the displacement of single boulders identified in the hillshaded DEMs. Several points were also located outside the rock glacier to assess the accuracy of the surface velocity determinations. Displacements in the horizontal plane were analysed instead of 3D displacements, which are affected by surface elevation changes (Isaksen et al., 2000).

:

4. Results

4.1 Accuracy assessment on the area of La Mare Glacier

The mean elevation difference between the SfM-MVS DEM from 4 September 2013 (Fig. 5a) and the ALS DEM from 22 September 2013 (Fig. 2b), evaluated in the common stable area outside the glacier, was -0.42 m (σ = 1.72 m). The same calculation between the SfM-MVS DEM from 27 September 2014 (Fig. 5b) and the ALS DEM from 24 September 2014 (Fig. 2a) yielded a mean value of 0.03 m (σ = 0.74 m). In this area, the mean difference between the 2014 and 2013 SfM-MVS DEMs is 0.38 m (σ = 1.73 m), and the mean difference between the respective ALS DEMs is -0.09 m (σ = 0.29 m, Table 3).

These results show that the photogrammetric survey conducted in 2014, using a higher number of camera positions and photographs and a slightly longer focal length, provided a significant improvement compared to the survey of 2013. In addition to the higher σ, the 2013 SfM-MVS DEM has a residual average bias of -0.42 m, which must be taken into account in the glacier mass balance calculations.

Table 3 ~~also~~ presents the same statistics for the area of the glacier. However, given that in 2013 the ablation was not negligible between the photogrammetric survey of 4 September and the ALS survey of 22 September, the comparison between SfM-MVS and ALS of the same year is meaningful only in 2014, with a mean difference of 0.23 m (σ = 0.65 m). The comparison of the two ALS DEMs of 2014 and 2013 yields a mean difference of 1.30 m for the glacier, attributable to the positive mass balance experienced by the glacier in that time period (+0.83 m w.e., Carturan, ~~2015~~2016).

The spatial distribution of the elevation difference between the SfM-MVS and ALS DEMs surveyed at the same times (Fig. 6 and 7) suggests that the most problematic areas for photogrammetric reconstructions are those that are far from the camera positions, steep, and covered by fresh snow. Certain outliers can be observed in steep areas outside the glaciers, even after filtering, but they likely have no influence on the glacier, where the slope is much lower.

The factors controlling the quality of the photogrammetric DEMs were investigated in detail u~~U~~sing the SfM-MVS DEM from 27 September 2014, which has a higher spatial coverage than that of 2013 and is almost contemporaneous with the ALS DEM from 24 September 2014 (which means negligible ablation and accumulation on the glacier).~~, we investigated in detail the factors controlling the quality of the photogrammetric DEMs.~~

As expected, the standard deviation of elevation differences between the 2014 SfM-MVS and ALS DEMs is proportional to slope but remains lower than 1 m up to 40° on the glacier and up to 60° in the area outside it (Fig. 8). Grouping the data for slope classes of 10 degrees and excluding classes with less than 1000 grid cells, it was possible to calculate a strong correlation between the absolute value of the elevation difference and the slope (R = 0.86 both inside and outside the glacier, significant at the 0.05 level). A rapid increase in the error is observed for the highest slope classes, which represent a very small part of the investigated area. For the glacier, only 1% of the area has a slope higher than 40°. The mean elevation difference is around zero for most of the low- and middle-slope classes, with the exception of the 0-10° class

inside the glacier, where a mean value of 0.41 m (σ = 0.44 m) was calculated. Interestingly, ~~T~~the majority of this slope class lies in a flat area of the glacier at 3200-3300 m a.s.l. and is covered by fresh snow, which has poor texture. In addition, this zone has an unfavourable line of sight from the camera positions.

~~We therefore investigated~~ ~~T~~the role of the incidence angle between the line of sight of the camera and the photographed object (vector normal to the surface), was investigated by analysing the mean angles calculated from five representative camera locations at different elevations. The analysis was performed for the glacier area, where most of the mean incidence angles ranges between 70° and 90° (75%, Figure 9a).~~As Figure 9a shows, more than 80%of the incidence angles in single pixels range between 70° and 90°.~~ The scatterplot ~~Figure (~~Fig 9c~~)~~ of elevation differences between the 2014 SfM-MVS and ALS DEMs ~~and~~versus the mean incidence angles calculated for ~~each~~every pixel shows no statistically significant relationship (R^2 = 0.~~045~~21). ~~between incidence angle and elevation difference~~However, by analysing this relationship for ~~intervals~~classes of incidence angle, and considering the mean of the ~~absolute value of~~ elevation differences in absolute value and the classes with more than 1000 pixels, yields a correlation coefficient R = 0.95 (significant at the 0.05 level).~~conf~~.~~irming the conclusions reached by Piermattei et al. (2015). Contrary to what was speculated, high mean and standard deviation values were obtained for low (i.e., theoretically favourable) incidence angles, which correspond to areas with high slope. Instead, low and approximately constant low standard deviation values were obtained for high incidence angles. These results suggest~~ that, in our case study, the accuracy of the SfM-MVS DEMs is influenced more by the slope than by the incidence angle.

Because ~~T~~the redundancy of the observations, that is~~ that means~~ the number of ~~camera that view~~cameras that views the same points on the glacier,~~ is a factor that~~ influences the quality of the photogrammetric results, a viewshed analysis was carried out (Fig. 9d).The results show~~ed~~ anti-correlation between the absolute value of elevation difference and the number of cameras viewing reconstructed pixels (Fig. 9e), yielding a coefficient of correlation of -0.63, which is significant at the 0.05 level.

The effect of the ~~Because the~~ camera-object distance (i.e., depth, ~~) strongly influences the photogrammetric accuracy (~~Gómez-Gutiérrez et al., 2014), ~~we evaluated its effect~~ was evaluated by calculating the mean and standard deviation of the elevation difference between the 2014 SfM-MVS and ALS DEMs, clustering the

pixels in 200 m distance classes from a camera position at the centre of the array displayed in Figure 4b. The relationship between error and depth is clearer for the glacier area (Fig. 10a), whereas in the surrounding area, the error appears to be more influenced by the variability of the slope angle (Fig. 10b).

~~The obtained results were compared to the theoretical behaviour of the error according to the Eq. 1. as a function of the depth (σ_d), as calculated using the following formulation:~~

~~$$\sigma_d = m_B \cdot \frac{D}{B} \cdot \sigma_i, \quad (1)$$~~

~~where m_B represents the image scale (*D / focal length*); *D* is the depth (camera-object distance); B is the baseline and σ_i is the measured accuracy in the image space.~~

The theoretical σ_d was calculated using Eq. 1 for each class of distance, considering a mean baseline of 400 m and an accuracy in the image space of 0.40 pixel, which is the reprojection error after bundle adjustment computations. Another quantification of the error as a function of the depth was obtained, for comparison purposes, by multiplying the Ground Sample Distance (GSD) (which increases with depth) by the reprojection error provided by PhotoScan for the Ground Control Points. Figure 10c shows that, on the glacier, the accuracy calculated from the DoD matches quite well the 'theoretical' calculations up to a depth of 1900 m. Beyond this distance, the detected error increases faster than in theory, likely due to the increasing coverage of fresh snow, which affects the image texture and decreases the accuracy.

~~We T~~The accuracy of photogrammetric reconstructions for the different substrata was then evaluated.~~,~~ The ~~whose~~ spatial distribution of each ~~substrata~~substratum was outlined on the orthophoto exported from PhotoScan. Debris, ice and firn display similar accuracy, with median values of elevation difference between the 2014 SfM-MVS and ALS-based DEMs close to zero and interquartile ranges of the same magnitude. Conversely, the area covered by fresh snow, which is also the area with greater depth, shows prevailing positive differences, a median value of 0.48 m and a much higher standard deviation (σ = 0.82 m).

The texture of the surface also influences the point density distribution and the spatial coverage of the reconstructed area. A lower value of the point density was obtained

for fresh snow (4 pts m^{-2}). Increasing point densities were obtained for firn, ice and debris (10, 13 and 15 pts m^{-2}, respectively).

The spatial coverage in the fresh snow area was 75%, whereas it was 93% in the rest of the glacier. Excluding the areas not visible from the camera position and occlusions imposed by the topography, the spatial coverage in the fresh snow area was 82% and 98% in the remaining part.

The point density is also affected by the depth, elevation and slope (Fig. 12). Due to the GSD, the average point density decreases with depth, which in our case is also proportional to the elevation. On the glacier, the point density decreases more rapidly than in the surrounding area for elevations between 3100 and 3300 m a.s.l ., due to the poor texture in this snow-covered flat area. Increasing densities with slope, up to 70-80°, are observed and likely result from more favourable incidence angles, which do not however guarantee high accuracy, as noted earlier (Fig. 9). Considering the entire reconstructed surface, the point density was higher in the area surrounding the glacier than on it (12 pts m^{-2} vs. 8 pts m^{-2}, respectively).

4.2 Accuracy assessment in the area of the AVDM3 Rock Glacier

The 2014 terrestrial photogrammetric survey of the AVDM3 Rock Glacier provided a good spatial coverage (83%) of high-resolution terrain data (Fig. 13). The spatial distribution of the elevation difference between the contemporaneous SfM-MVS and ALS DEMs shows the existence of areas with both positive and negative values (Fig. 14). The average elevation difference is 0.02 m on the rock glacier (σ = 0.17) and 0.05 in the surrounding areas (σ = 0.31 m, Tab. 5).

Similar to the La Mare Glacier area, the accuracy decreases with increasing slope in the rock glacier area. The standard deviation of the average elevation difference between the SfM-MVS and ALS DEMs is less than 0.20 m up to 40°. In the area surrounding the rock glacier, the error increases faster with slope because steep areas coincide with shaded areas and (because the images were acquired in the afternoon) high solar zenith angles. As suggested by Gómez-Gutiérrez et al., (2014), ~~we calculated~~ the relationship between the quality of the photogrammetric DEM and the amount of shadowed-lighted areas in the photographs was calculated~~,~~ using a hillshaded model that was calculated by simulating the position of the sun in the sky (azimuth and zenith angles) during the survey. As shown in Figure 16, larger errors

occur in shadowed areas and smaller errors in well-lit areas, even if the largest differences in accuracy can be observed outside rather than on the rock glacier.

4.3 Glacial and periglacial processes

4.3.1 Mass balance ~~calculations of~~on ~~on~~ La Mare Glacier

Due to abundant solid precipitation during the accumulation season and low ablation rates during the summer (the glacier was snow-covered above ~3000-3100 m a.s.l.), the mass balance of the La Mare Glacier was positive in the 2013-14 hydrological year for the first time since the beginning of measurements in 2003. ~~At the end of the ablation season, the Equilibrium Line Altitude (ELA) was at 3012 m a.s.l., and the Accumulation Area Ratio (i.e., the ratio between the accumulation area and the total area, AAR) was 0.86.~~ According to the direct glaciological method, the annual mass balance was +0.83 m w.e. (Carturan, ~~2015~~2016).

~~We compared mass balance estimates obtained was calculated according to the Eq. 3 with the geodetic method based onfor the SfM-MVS and ALS DEMs acquired in 2013 and 2014 and the results was compared. The geodetic mass balance was calculated from the total volume change ΔV (m^3) between the two survey dates:~~

~~$V = \overline{\Delta z} \cdot A$ (2)~~

~~where $\overline{\Delta z}$ is the average elevation change between two DEMs over the area A of the glacier. The area-averaged net geodetic mass balance in metres of water equivalent per year (m w.e. y^{-1}) was calculated as~~

~~$\dot{M} = \frac{\Delta V \cdot \rho}{A}$ (3)~~

~~where ρ is the mean density. The area A of the glacier between the two surveys did not change. The mean density was obtained by a fractional area-weighted mean, assigning 900 kg/m^3 for the ablation area (Huss, 2013) and 530 kg/m^3 for the accumulation area, as directly measured in a snowpit. The resulting weighted mean density was 600 kg/m^3. In the mass balance calculations, we used both raw $\overline{\Delta z}$ values and corrected $\overline{\Delta z}$ valuesto account for the mean errors in the stable areas outside the glacier, as reported in Table 3.~~

As shown in Table 4, the geodetic mass balance estimates using only ALS data do not differ significantly for either the entire glacier or the sub-areas covered by the photogrammetric surveys of 2013 and 2014 (88% and 93%, respectively). The

485 estimates range between 0.85 and 0.88 m w.e for the raw data and between 0.90
486 and 0.94 m w.e. for the corrected data. The geodetic mass balance calculations
487 using only photogrammetric data yield a raw value of 1.09 m w.e. and a corrected
488 value of 0.87 m w.e. Using the 2014 SfM-MVS, which has a higher quality than the
489 2013 ALS DEM, yields a raw value of 0.98 m w.e. and a corrected value of 1.02 m
490 w.e. Area-averaged estimates of the geodetic mass balance from photogrammetric
491 data are very close to the estimates from ALS data and from the direct method and
492 are closer still if the mean DEM error in the stable areas outside the glacier is
493 subtracted from the raw average elevation differences. The spatial distribution and
494 magnitude of elevation change is also well captured by the terrestrial
495 photogrammetry (Fig. 17 and 18), even if, as already noted in the previous section,
496 problematic areas are present in the upper part of the glacier, which was covered by
497 fresh snow, especially in the 2013 SfM-MVS survey.

498

499 **4.3.2 Surface changes and velocities of the AVDM3 Rock Glacier**

500 The spatial distribution and the mean value of elevation change on the surface of the
501 AVDM3 Rock Glacier were calculated differencing the available SfM-MVS and ALS
502 DEMs. Table 5 shows that, according to the ALS data, there was a prevailing
503 lowering of the surface in the period from 2003 to 2014. Taking into account the
504 average residual bias in the stable area outside the rock glacier, the average
505 lowering rates of the rock glacier surface were 1.5 cm y^{-1} in the period from 2003 to
506 2013, and 2 cm in the year 2013-14. Comparing the SfM-MVS DEM of 2014 with the
507 ALS DEMs of 2013 and 2003 and accounting for the mean bias outside the rock
508 glacier, we obtained slightly higher lowering rates of 2.2 cm y^{-1} from 2003 to 2013
509 and 5 cm from 2013 to 2014. As expected on the basis of the accuracy assessment
510 (Section 4.2), the decadal lowering rates calculated from the SfM-MVS DEM are in
511 closer agreement with those calculated from ALS data than the single-year
512 calculations. The same can be observed for the spatial distribution of the elevation
513 changes (Fig. 19), which shows a prevailing thinning in the upper and middle part of
514 the rock glacier and a thickening of the two advancing lobes.
515 ~~Based on these results, we compared the surface displacement rates (based on~~
516 ~~photogrammetric and ALS data) for the period from 2003 to 2014. We usedby a~~
517 ~~manual measurements of the displacement of single boulders identified in the~~

~~hillshaded DEMs. Several points were also located outside the rock glacier to assess the accuracy of the surface velocity determinations.~~

Figure 20 shows that the fastest moving areas in the period from 2003 to 2014 ~~are~~ were the two frontal lobes, which also featured the greatest elevation changes. Table 6 shows that the SfM-MVS and ALS data produced very similar surface velocities for the three sub-areas (each with homogeneous displacement) into which the rock glacier can be divided. Outside the rock glacier, the photogrammetric method exhibited a slightly lower accuracy compared to the ALS, but no systematic shift of the different DEMs was found.

5. Discussion

5.1 Data processing and accuracy assessments

The results of our terrestrial photogrammetry applications on the La Mare Glacier and on the AVDM3 Rock Glacier demonstrate that it is possible to reliably quantify the investigated glacial and periglacial processes by means of a quick and safe survey that was conducted on a single day using cheap, light and easy-to-use hardware. Moreover, time-consuming and unsafe direct access to the glacier surface was not required.

T~~However, t~~he data processing times were significantly long~~er~~. For a single operator, the processing time is approximately 10 days. The most labour-intensive and time-consuming tasks were the pre-processing steps i.e., masking of the photos, identification of reference points from the LiDAR DEM and then in the images, and processing of the images (the MVS step is particularly computationally intensive), which is directly related to the resolution and the number of photographs uploaded and the computer performance. Several steps required a certain degree of subjectivity, e.g., the identification of the GCPs. However, due to the high automatism of the image processing, the level of expertise is considerably lower than for LiDAR and traditional photogrammetry.

On the La Mare Glacier, the area-averaged estimates of the 2013-14 geodetic mass balance from ALS and photogrammetric data were almost identical (0.91 and 0.87 m w.e., respectively) and close to the mass balance calculated from the direct

glaciological method (0.83 m w.e.). The differences are well within the uncertainty of the direct mass balance estimates, which was quantified in 0.26~~has been quantified as approximately ±0.2~~ m w.e. y^{-1} by ~~previous studies (Cogley and Adams, 1998; Cogley, 2009)~~Carturan (2016). These results confirm that the good results obtained by Piermattei et al., (2015) on the small Montasio Glacier, in the Julian Alps, can also be replicated on larger glaciers with different morphologies and characteristics.

Because the AVDM3 Rock Glacier exhibited quite slow annual deformation and creep, we were able to calculate reliable displacement rates and area-averaged surface elevation changes only on a multi-year (in our case, decadal) time scale. This result confirms the findings of Gómez-Gutiérrez et al. (2014), who applied a similar method to the Corral del Veleta Rock Glacier in the Sierra Nevada (Spain).

Our results are promising, despite the limitations of the adopted method, which include i) the location of GCPs on natural targets outside the investigated glacier/rock glacier, ii) the presence of areas with deep shadows and changes in the light during the survey, iii) the presence of fresh snow in the upper and middle part of the glacier, and iv) the high camera-object distance in the glacier application.

In general terms, the photo-based accuracy is related to the image feature extraction, feature matching (in both the SfM and MVS steps), and scale definition (Bemis et al., 2014). A low accuracy in these steps, caused for example by poor camera network geometry, can generate model distortion and reduce the ability to identify unique corresponding features in overlapping images (Wackrow and Chandler, 2011; Dall`Asta et al., 2015~~b~~, Favalli et al., 2012; James and Robson, 2012; 2014; Hosseininaveh et al, 2014; Micheletti et al., 2014; Nocerino et al., 2014). In our case studies, among the various aspects analysed, the spatial variability of the accuracy of the photogrammetric DEMs is related to the camera-object distance, the presence of fresh snow with low contrast, the changing illumination during the survey and the occurrence of shadows. The increasing error with increasing terrain slope suggests the persistence of a small shift in the reconstructed DEMs. This shift, however does not affect the areal estimates of mass balance and elevation change, given that the vast majority of the glacier and rock glacier areas feature small or moderate slope angles. For both the glacier and the rock glacier, the spatial coverage of the reconstructed areas was not complete.~~, we have not obtained complete spatial coverage was obtained.~~ In the glacier surveys, the problematic areas were those not visible from the camera positions and those covered by fresh snow and far from the

viewpoints. In the rock glacier, certain areas were not reconstructed due to the rock glacier's complex morphology and in particular to the presence of ridges, furrows and counterslopes.

5.2 ~~Recommendations~~Possible improvements of the SfM-MVS approach

~~Our~~ The accuracy assessments confirm that the ALS data still provide results with somewhat higher accuracies (Tabs. 3 and 5, Figs. 6 and 14) but with much higher costs and demanding logistics than the SfM-MVS approach. However, the SfM-MVS method has the potential to provide a significantly higher spatial resolution (Debella-Gilo and Kaab, 2011; Piermattei et al., 2015) and temporal resolution due to its significantly lower costs. Moreover, the photogrammetric reconstructions still have room for improvement, as demonstrated by the better results achieved from the 2014 survey of the glacier area compared to those from 2013. This improvement resulted from a higher number of photographs and improved camera network geometry.

Many of the limitations described above can be overcome by introducing modifications to the terrestrial photogrammetric survey strategy. For the rock glacier survey, shorter baselines are recommended to ensure greater spatial coverage, high image similarity and good matching performance (Wenzel et al., 2013). GCPs, for example, could be placed on the surface of the glaciers and rock glaciers to reduce the model distortions (Bemis et al., 2014) and generate surveys with much higher accuracies via, for example, the use of dGPS (Dall'Asta et al., 2015~~a~~).

The use of ~~Unmanned Aerial Vehicles (~~UAVs~~)~~ could solve the problem of excessive camera-object distances and the issue of missing areas due to inaccessibility. However, these alternatives imply increased costs, more troublesome logistics, greater expertise, and ultimately longer survey times. In addition, they also require directly accessing unsafe or difficult to reach areas, both to place targets and to move UAVs among study areas that exceed their operational range (Bühler et al., 2014). Therefore, the best balance must be found between simplicity, safety, costs and accuracy for each photogrammetric application based on the final objectives and on the available human and economic resources.

6. Conclusions

In this paper, we investigated the applicability of the SfM-MVS approach for monitoring glacial and periglacial processes in a catchment of the Ortles-Cevedale Group (Eastern Italian Alps), validating our results using ALS DEMs as benchmarks. The ground surveys were conducted on foot and were intentionally planned to be as quick and easy as possible. ~~We surveyed~~ T~~t~~he 2.1 ~~-~~km^2 La Mare Glacier and the neighbouring AVDM3 Rock Glacier were surveyed in one day using only a consumer-grade SLR camera without the setup of artificial targets.

The accuracy of the photogrammetric DEMs, evaluated as the mean and standard deviation of the elevation difference in a stable area between the SfM-MVS DEM and the reference ALS DEM, was -0.42 m ± 1.72 m and 0.03 m ± 0.74 m for the 2013 and 2014 surveys, respectively. The SfM-MVS DEM accuracy of the reconstructed rock glacier surface acquired in 2014 was estimated to be 0.02 m ± 0.17 m.

The SfM-MVS geodetic mass balance estimates for the La Mare Glacier were in good agreement with the calculations from the contemporary ALS data and with the results of the direct glaciological method, confirming a positive mass balance of approximately 0.9 m w.e. in the 2013-14 hydrological year. In the rock glacier, the ~~expeditious~~ survey produced a good spatial coverage of the photogrammetric DEM and a reliable calculation of the multi-year surface changes and displacement rates. For rock glacier applications, particularly for slow-mowing ones such as AVDM3, single-year assessments of elevation change and surface velocities require the setup of artificial targets and GCPs to obtain the accuracy required to detect such slow processes.

The simplicity of the ground surveys and the physical characteristics of the analysed alpine terrain were the main factors influencing the tested approach. In particular, we refer to the use of natural targets as GCPs, the occurrence of shadowed areas and lighting changes during the surveys, the presence of fresh snow in the upper part of the glacier (which reduced the contrast), and the sub-optimal camera network geometry and long camera-object distances imposed by the morphology and accessibility of the study area.

In consideration of the factors that spatially control the accuracy of the SfM-MVS DEMs, there remains room for significant improvements, e.g., using ~~UAVs~~ aerial platform and/or placing artificial targets surveyed by dGPS. Further research is therefore needed to i) find technical solutions to overcome the major limitations of the SfM-MVS approach in such remote areas and ii) achieve the optimal balance

between the simplicity and low cost of this approach and the accuracy required for each specific application.

Acknowledgments

This study was funded by the Italian MIUR Project (PRIN 2010-11): 'Response of morphoclimatic system dynamics to global changes and related geomorphological hazards' (local and national coordinators G. Dalla Fontana and C. Baroni). The authors would like to thank Philipp Glira from the TU of Wien for his precious contribution to the LiDAR data processing. The comments and suggestions from Susan Conway, Álvaro Gómez-Gutiérrez and an anonymous Reviewer have been useful for the improvement of the manuscript.

References

~~Abermann, J., Fischer, A., Lambrecht, A., and Geist, T.: On the potential of very high-resolution repeat DEMs in glacial and periglacial environments, The Cryosphere, 4, 53–65, doi:10.5194/tc-4-53-2010, 2010.~~

AgiSoft LL C: AgiSoft PhotoScan Professional Edition. Version 1.1.2, available at: http://www.agisoft.ru/products/photoscan/ (last access: 18 January 2015), 2010a.

AgiSoft LL C: AgiSoft PhotoScan User-manuals Version 1.0, available at: http://www.agisoft.com/pdf/photoscan-pro_1_1_en.pdf (last access: 15 May 2015), 2010b.

~~Aguilar, F. J. and Mills, J.: Accuracy assessment of lidar-derived digital elevation models, Photogramm. Rec., 23, 148–169, 2008.~~

~~Ahn, Y. and Box, J., E.: Glacier velocities from time-lapse photos: technique development and first results from the Extreme Ice Survey (EIS) in Greenland. J. Glaciol., 56, 723–734, 2010.~~

~~Baltsavias, E. P., Favey, E., Bauder, A., Bosch, H., and Pateraki, M.: Digital surface modelling by airborne laser scanning and digital photogrammetry for glacier monitoring, Photogramm. Rec., 17, 243–273, doi:10.1111/0031-868X.00182, 2001.~~

679 Bemis, S., Micklethwaite, S., and Turner, D.: Ground-based and UAV-Based
680 photogrammetry: a multi-scale, high-resolution mapping tool for Structural Geology
681 and Paleoseismology. J Struct Geol., 69, 163–178, doi:10.1016/j.jsg.2014.10.007,
682 2014.

683 Bertone, A.: Misure di spostamento dei rock glacier con l'uso di feature tracking
684 applicato a DTM multitemporali, BSc Thesis, Department of Earth and Environmental
685 Sciences, University of Pavia, Pavia, Italy, 63 pp., 2014.

686 Besl, P. J. and McKay, N. D.: Method for registration of 3-D shapes, in: Proceedings
687 of the International Society for Optics and Photonics IEEE Transactions on Pattern
688 Analysis and Machine Intelligence, 1611, 586–606, 1992.

689 Bradley, D., Boubekeur, T., and Heidrich, W.: Accurate multi-view reconstruction
690 using robust binocular stereo and surface meshing, in: IEEE Conference on
691 Computer Vision and Pattern Recognition, Anchorage, AK, USA, 1–8, 2008.

692 ~~Bühler, Y. and Graf, C.: Sediment transfer mapping in a high-alpine catchment using~~
693 ~~airborne LiDAR. GRAF, C.(Red.) Mattertal – ein Tal in Bewegung, Publikation zur~~
694 ~~Jahrestagung der Schweizerischen Geomorphologischen Gesellschaft, 29 June–1~~
695 ~~July 2011, Eidg. Forschungsanstalt WSL, St. Niklaus, Birmensdorf, Switzerland, 113–~~
696 ~~124, 2013.~~

697 Bühler, Y., Marty, M., Egli, L., Veitinger, J., Jonas, T., Thee, P., and Ginzler, C.:
698 Spatially continuous mapping of snow depth in high alpine catchments using digital
699 photogrammetry, The Cryosphere Discuss., 8, 3297–3333, doi:10.5194/tcd-8-3297-
700 2014, 2014.

701 Carturan, L.: Climate change effects on the cryosphere and hydrology of a high-
702 altitude watershed, PhD thesis, Department of Land, Environment, Agriculture and
703 Forestry, University of Padova, Padova, Italy, 2010.

704 Carturan, L.: Replacing monitored glaciers undergoing extinction: a new
705 measurement series on La Mare Glacier (Ortles-Cevedale, Italy)~~Starting new mass~~
706 ~~balance observations close to decaying monitored glaciers: La Mare Glacier (Ortles-~~
707 ~~Cevedale, Italian Alps)~~, J. Glaciol., in ~~preparation~~review, ~~2015~~2016.

Carturan, L., Cazorzi, F., and Dalla Fontana, G.: Enhanced estimation of glacier mass balance in unsampled areas by means of topographic data, Ann. Glaciol., 50, 37–46, 2009.

Carturan, L., Baldassi, G., Bondesan, A., Calligaro, S., Carton, A., Cazorzi, F., Dalla Fontana, G., Francese, R., Guarnieri, A., Milan, N., Moro, D., Tarolli, P.: Current behavior and dynamics of the lowermost italian glacier (Montasio Occidentale, Julian Alps), Geografiska Annaler: Series A, Physical Geography, 95, 79–96, 2013.

Carturan, L., Baroni, C., Carton, A., Cazorzi, F., Fontana, G. D., Delpero, C., and Zanoner, T.: Reconstructing Fluctuations of La Mare Glacier (Eastern Italian Alps) in the Late Holocene: new Evidence for a Little Ice Age Maximum Around 1600 AD. Geografiska Annaler: Series A, Physical Geography, 96, 287–306, 2014.

Carturan, L., Zuecco, G., Seppi, R., Zanoner, Z., Borga, M., Carton, A., and Dalla Fontana, G.: Catchment-scale permafrost mapping using spring water characteristics, Permafrost Periglac., in press, doi: 10.1002/ppp.1875, 2015.

Chen, Y. and Medioni, G.: Object modeling by registration of multiple range images, in: Proceedings, IEEE International Conference on Robotics and Automation, 9–11 April, Sacramento, CA, USA, 10, 145–155, 1991.

~~Clapuyt, F., Vanacker, V., and Van Oost, K.: Reproducibility of uav-based earth topography reconstructions based on structure-from-motion algorithms, Geomorphology, doi:10.1016/j.geomorph.2015.05.011, 2015.~~

~~Cogley, J. G.: Geodetic and direct mass-balance measurements: comparison and joint analysis, Ann. Glaciol., 50, 96–100, 2009.~~

~~Cogley, J. G. and Adams, W. P.: Mass balance of glaciers other than the ice sheets, J. Glaciol, 44, 315–325, 1998.~~

~~Colucci, R. R., Forte, E., Boccali, C., Dossi, M., Lanza, L., Pipan, M., and Guglielmin, M.: Evaluation of internal structure, volume and mass of glacial bodies by integrated LiDAR and ground penetrating radar surveys: the case study of Canin Eastern Glacieret (Julian Alps, Italy), Surv. Geophys., 36, 231–252, 2015.~~

Dall'Asta, E., Delaloye, R., Diotri, F., Forlani, G., Fornari, M., Morra di Cella, U., Pogliotti, P., Roncella, R., Santise, M.: Use of UAS in a high mountain landscape: the

738 case of gran sommetta rock glacier (AO), The International Archives of the
739 Photogrammetry, Remote Sensing and Spatial Information Sciences, Volume XL-
740 3/W3, 391–397, 2015a.

741 Dall'Asta, E., Thoeni, K., Santise, M., Forlani, G., Giacomini, A., and Roncella, R.:
742 Network design and quality checks in automatic orientation of close-range
743 photogrammetric blocks, Sensors, 15, 7985–8008, 2015b.

744 Debella-Gilo, M. and Kääb, A.: Sub-pixel precision image matching for measuring
745 surface displacements on mass movements using normalized cross-correlation.
746 Remote Sens. Environ., 115, 130–142, 2011.

747 Deems, J. S., Painter, T. H., and Finnegan, D. C.: Lidar measurement of snow depth:
748 a review, J. Glaciol., 59, 467–479, 2013.

749 Favalli, M., Fornaciai, A., Isola, I., Tarquini, S., and Nannipieri, L.: Multiview 3D
750 reconstruction in geosciences, Comput. Geosci., 44, 168–176, 2012.

751 Fischer, L., Eisenbeiss, H., Kääb, A., Huggel, C., and Haeberli, W.: Monitoring
752 topographic changes in a periglacial high-mountain face using high-resolution DTMs,
753 Monte Rosa East Face, Italian Alps, Permafrost Periglac., 22, 140–152, 2011.

754 Gauthier, D., Conlan, M., and Jamieson, B.: Photogrammetry of fracture lines and
755 avalanche terrain: potential applications to research and hazard mitigation projects,
756 Proceedings, International Snow Science Workshop, Banff, 29 September–3 October
757 2014, 109–115, 2014.

758 Geist, T. and Stotter, J.: Documentation of glacier surface elevation change with multi
759 temporal airborne laser scanner data – case study: Hintereisferner and
760 Kesselwandferner, Tyrol, Austria, Zeitschrift fur Gletscherkunde und Glazialgeologie,
761 41, 77–106, 2007.

762 Glira, P., Pfeifer, N., Briese, C., Ressl, C.: A correspondence framework for ALS strip
763 adjustments based on variants of the ICP algorithm, Photogramm. Fernerkun., 4,
764 275–289, doi:10.1127/pfg/2015/0270, 2015.

765 Gómez-Gutiérrez, Á., de Sanjosé-Blasco, J. J., de Matías-Bejarano, J., and
766 Berenguer-Sempere, F.: Comparing two photo-reconstruction methods to produce

high density point clouds and DEMs in the Corral del Veleta Rock Glacier (Sierra Nevada, Spain), Remote Sensing, 6, 5407–5427, 2014.

Gómez-Gutiérrez, Á., de Sanjosé-Blasco, J. J., Lozano-Parra, J., Berenguer-Sempere, F., and de Matías-Bejarano, J.: Does HDR pre-processing improve the accuracy of 3D models obtained by means of two conventional SfM-MVS software packages? The case of the Corral del Veleta Rock Glacier, Remote Sensing, 7, 10269–10294, 2015.

Hartley, R. and Zisserman, A.: Multiple View Geometry In Computer Vision, Cambridge University Press, Cambridge, UK, 2003.

Haeberli, W.: Creep of mountain permafrost: internal structure and flow of alpine rock glaciers, Mitteilungen der Versuchsanstalt für Wasserbau, Hydrologie und Glaziologie der ETH Zurich, 77, 5–142, 1985.

~~Haug, T., Rolstad, C., Elvehøy, H., Jackson, M., and Maalen-Johansen, I.: Geodetic mass balance of the western Svartisen ice cap, Norway, in the periods 1968–1985 and 1985–2002, Ann. Glaciol., 50, 119–125, 2009.~~

~~Höfle, B., Geist, T., Rutzinger, M., and Pfeifer, N.: Glacier surface segmentation using airborne laser scanning point cloud and intensity data, International Archives of Photogrammetry, Remote Sensing and Spatial Information Sciences, 36, W52, 195–200, 2007.~~

~~Höfle, B., and Rutzinger, M.: Topographic airborne LiDAR in geomorphology: A technological perspective. Zeitschrift für Geomorphologie, Supplementary Issues, 55(2), 1-29, 2011.~~

Hosseininaveh, A., Sargeant, B., Erfani, T., Robson, S., Shortis, M., Hess, M., and Boehm, J.: Towards fully automatic reliable 3D acquisition: from designing imaging network to a complete and accurate point cloud, Robotics and Autonomous Systems, 62, 1197–1207, 2014.

Huss, M.: Density assumptions for converting geodetic glacier volume change to mass change, The Cryosphere, 7, 877-887, doi:10.5194/tc-7-877-2013, 2013.

Immerzeel, W. W., Kraaijenbrink, P. D. A., Shea, J. M., Shrestha, A. B., Pellicciotti, F., Bierkens, M. F. P., and De Jong, S. M.: High-resolution monitoring of Himalayan

glacier dynamics using unmanned aerial vehicles, Remote Sens. Environ., 150, 93–103, 2014.

Isaksen, K., Ødegård, R. S., Eiken, T., and Sollid, J. L.: Composition, flow and development of two tongue-shaped rock glaciers in the permafrost of Svalbard. Permafrost and Periglacial Processes, 11, 241-257, 2000.

James, M. R. and Robson, S.: Straightforward reconstruction of 3D surfaces and topography with a camera: accuracy and geoscience application, J. Geophys. Res.-Earth, 117, F03017, doi:10.1029/2011JF002289, 2012.

James, M. R. and Robson, S.: Mitigating systematic error in topographic models derived from UAV and ground-based image networks, Earth Surf. Proc. Land. 39, 1413–1420, doi:10.1002/esp.3609, 2014.

~~Joerg, P. C. and Zemp, M.: Evaluating Volumetric Glacier Change Methods Using Airborne Laser Scanning Data. Geografiska Annaler: Series A, Physical Geography, 96, 135–145, 2014.~~

Kääb, A.: Monitoring high-mountain terrain deformation from repeated air-and spaceborne optical data: examples using digital aerial imagery and ASTER data. ISPRS Journal of Photogrammetry and remote sensing, 57, 39–52, 2002.

Kääb, A.: Remote Sensing of Mountain Glaciers and Permafrost Creep. Research Perspectives from Earth Observation Technologies and Geoinformatics, Schriftenreihe Physische Geographie, Glaziologie und Geomorphodynamik, 48, University of Zurich, Zurich, Switzerland, 2005.

~~Kääb, A. and Funk, M.: Modelling mass balance using photogrammetric and geophysical data: a pilot study at Griesgletscher, Swiss Alps. J. Glaciol. 45, 575–583, 1999.~~

~~Kääb, A., Haeberli, W., and Gudmundsson, G. H.: Analyzing the creep of mountain permafrost using high precision aerial photogrammetry: 25 years of monitoring Gruben rock glacier, Swiss Alps, Permafrost Periglac., 8, 409–426, 1997.~~

Kääb, A., Kaufmann, V., Ladstädter, R., and Eiken, T.: Rock glacier dynamics: implications from high-resolution measurements of surface velocity fields, in: Eighth

International Conference on Permafrost, 21–25 July 2003, Zurich, Switzerland, Vol. 1, 501–506, 2003.

Kääb, A., Girod, L., and Berthling, I.: Surface kinematics of periglacial sorted circles using structure-from-motion technology, The Cryosphere, 8, 1041–1056, doi:10.5194/tc-8-1041-2014, 2014.

~~Kaufmann, V.: Deformation analysis of the Doesen rock glacier (Austria), in: Proceedings of the 7th International Permafrost Conference, 23–27 June 1998, Yellowknife, Canada, 551–556, 1998.~~

~~Kaufmann, V. and Ladstädter R.: Application of terrestrial photogrammetry for glacier monitoring in Alpine environments, Proceedings of the 21st Congress of ISPRS, Beijing, China, 3–11 July 2008, Vol. 37, Part B8, 813–818, 2008.~~

~~Knoll, C. and Kerschner, H.: A glacier inventory for South Tyrol, Italy, based on airborne laserscanner data, Ann. Glaciol., 50, 46–52, 2010.~~

~~Kodde, M. P., Pfeifer, N., Gorte, B. G. H., Geist, T., and Höfle, B.: Automatic glacier surface analysis from airborne laser scanning, International Archives of the Photogrammetry, Remote Sensing and Spatial Information Sciences, 36, 221–226, 2007.~~

~~Maas, H. G., Schwalbe, E., Dietrich, R., Bässler, M., and Ewert, H.: Determination of spatiotemporal velocity fields on glaciers in West-Greenland by terrestrial image sequence analysis, International Archives of Photogrammetry, Remote Sensing and Spatial Information Science, 37, 1419–1424, 2008.~~

Micheletti, N., Chandler, J. H., and Lane, S. N.: Investigating the geomorphological potential of freely available and accessible Structure-from-Motion photogrammetry using a smartphone, Earth Surf. Proc. Land., 40, 473–486, doi:10.1002/esp.3648, 2014.

~~Müller, J., Gärtner-Roer, I., Thee, P., and Ginzler, C.: Accuracy assessment of airborne photogrammetrically derived high-resolution digital elevation models in a high mountain environment. ISPRS Journal of Photogrammetry and Remote Sensing, 98, 58–69, 2014.~~

Nilosek, D., Sun, S., and Salvaggio, C.: Geo-accurate model extraction from three-dimensional image-derived point clouds, in: Proceedings of SPIE, Algorithms and Technologies for Multispectral, Hyperspectral, and Ultraspectral Imagery XVIII, 23 April 2012, Baltimore, MD, USA, 8390, 83900J, doi:10.1117/12.919148, 2012.

Nocerino, E., Menna, F., and Remondino, F.: Accuracy of typical photogrammetric networks in cultural heritage 3D modeling projects, ISPRS-International Archives of the Photogrammetry, Remote Sensing and Spatial Information Sciences, 1, 465–472, 2014.

~~Pellikka, P. and Rees, W. G.: Remote Sensing Of Glaciers: Techniques For Topographic, Spatial and Thematic Mapping of Glaciers, CRC Press, University of Cambridge, Cambridge, UK, 2009.~~

Piermattei, L., Carturan, L., and Guarnieri, A.: Use of terrestrial photogrammetry based on structure from motion for mass balance estimation of a small glacier in the Italian Alps, Earth Surf. Proc. Land., 40, 1791–1802, doi:10.1002/esp.3756, 2015.

~~Prosdocimi, M., Sofia, G., Dalla Fontana, G., Tarolli, P.: Bank erosion in agricultural drainage networks: effectiveness of Structure-from-Motion for post-event analysis, Earth Surf. Proc. Land., 40, 1891–1906, doi:10.1002/esp.3767, 2015.~~

Ryan, J. C., Hubbard, A. L., Box, J. E., Todd, J., Christoffersen, P., Carr, J. R., Holt, T. O., and Snooke, N.: UAV photogrammetry and structure from motion to assess calving dynamics at Store Glacier, a large outlet draining the Greenland ice sheet, The Cryosphere, 9, 1–11, doi:10.5194/tc-9-1-2015, 2015.

Roer, I. and Nyenhuis, M.: Rockglacier activity studies on a regional scale: comparison of geomorphological mapping and photogrammetric monitoring, Earth Surf. Proc. Land., 32, 1747–1758, 2007.

Seppi, R., Carton, A., Zumiani, M., Dall'Amico, M., Zampedri, G., and Rigon, R.: Inventory, distribution and topographic features of rock glaciers in the southern region of the Eastern Italian Alps (Trentino). Geografia Fisica e Dinamica Quaternaria 35, 185–197, doi:10.4461/GFDQ.2012.35.17, 2012.

~~Shenk, T.: Digital Photogrammetry Vol. 1, Terra Science, Laurelville, OH, USA, 1, 43135, 428 pp., 1999.~~

885 Solbø, S. and Storvold, R.: Mapping svalbard glaciers with the cryowing uas, ISPRS
886 International Archives of the Photogrammetry, Remote Sensing and Spatial
887 Information Sciences, XL-1/W2, 373–377, 2013.

888 ~~Stumpf, A., Malet, J. P., Allemand, P., Pierrot-Deseilligny, M., and Skupinski, G.:~~
889 ~~Ground-based multi-view photogrammetry for the monitoring of landslide deformation~~
890 ~~and erosion, Geomorphology, 231, 130–145, 2015.~~

891 ~~Tarolli, P.: High-resolution topography for understanding Earth surface processes:~~
892 ~~opportunities and challenges, Geomorphology, 216, 295–312, 2014.~~

893 Tonkin, T. N., Midgley, N. G., Graham, D. J., and Labadz, J. C.: The potential of
894 small unmanned aircraft systems and structure-from-motion for topographic surveys:
895 a test of emerging integrated approaches at Cwm Idwal, North Wales,
896 Geomorphology, 226, 35–43, 2014.

897 Tseng, C.-M., Lin, C. W., Dalla Fontana, G., Tarolli, P.: The topographic signature of
898 a Major Typhoon, Earth Surf. Proc. Land., 40, 1129–1136, 2015.

899 Verhoeven, G., Karel, W., 'tuhec, S., Doneus, M., Trinks, I., and Pfeifer, N.: Mind your
900 grey tones – examining the influence of decolourization methods on interest point
901 extraction and matching for architectural image-based modelling, in: 3D-Arch 2015–
902 3D Virtual Reconstruction and Visualization of Complex Architectures (ISPRS WG
903 V/4, CIPA), 25–27 February 2015, Vol. 40, ISPRS, Avila, Spain, 307–314, 2015.

904 Wackrow, R. and Chandler, J.: Minimising systematic error surfaces in digital
905 elevation models using oblique convergent imagery, Photogramm. Rec., 26, 16–31,
906 2011.

907 ~~Welch, R., and Howarth, P. J.: Photogrammetric measurements of glacial landforms,~~
908 ~~Photogramm. Rec., 6, 75–96, doi:10.1111/j.1477–9730.1968.tb00915.x, 1968.~~

909 Wenzel, K., Rothermel, M., Fritsch, D., and Haala, N.: Image acquisition and model
910 selection for multi-view stereo, Int. Arch. Photogramm. Remote Sens. Spatial Inf. Sci,
911 251–258, 2013.

912 Whitehead, K., Moorman, B. J., and Hugenholtz, C. H.: Brief Communication: Low-
913 cost, ondemand aerial photogrammetry for glaciological measurement, The
914 Cryosphere, 7, 1879–1884, doi:10.5194/tc-7-1879-2013, 2013.

~~Whitehead, K., Moorman, B., and Wainstein, P.: Instruments and Methods Measuring daily surface elevation and velocity variations across a polythermal arctic glacier using ground based photogrammetry, J. Glaciol., 60, 1208–1220, doi:10.3189/2014JoG14J080, 2014.~~

Zemp, M., Thibert, E., Huss, M., Stumm, D., Denby, C. R., Nuth, C., Nussbaumer, S. U., Moholdt, G., Mercer, A., Mayer, C., Joerg, P. C., Jansson, P., Hynek, B., Fischer, A., Escher-Vetter, H., Elvehøy, H., and Andreassen, L. M.: Reanalysing glacier mass balance measurement series. The Cryosphere, 7, 1227-1245, doi:10.5194/tc-7-1227-2013, 2013.

940 **Table 1**. Date and main parameters of available LiDAR data.

Date	Aircraft	Laser scanner model	Laser scanner rate	Max. scan angle	Scan frequency	Point density [pts·m^{-2}]
24 Sept. 2014	Elicopter AS350 B3	Optech ALTM GEMINI (04SEN164)	100 kHz	46°	34 Hz	5.1
22 Sept. 2013	Cessna 404 D-IDOS	ALTM 3100	70,000 Hz	±25°	32 Hz	0.9
17 Sept. 2003	—	—	—	—	—	0.5

941

942 **Table 2**. Data acquisition settings and processing results of the photogrammetric
943 surveys for both case studies. The GCPs error is the average transformation
944 residuals error [m] and root mean square reprojection error for the GCPs [pix] during
945 the bundle adjustment computation. The image quality represents the downsized of
946 the images resolution during the dense matching computation. “Ultra high” means full
947 resolution, “High” a downsized of 50% before the image matching processing. The
948 ground sample distance (GSD) is the average pixel size on the ground. The standard
949 deviation of ICP registration is reported in the table.

	La Mare glacier		**Rock glacier**
	4 September 2013	27 September 2014	27 September 2014
Input data			
Camera type	Nikon 600D	Nikon 600D	Canon 5D Mark III
Focal Length	25 mm	35 mm	28 mm
Image size	5184 x 3456 pix	5184 x 3456 pix	5760 x 3840 pix
N° Images	37	177	198
Processing data			
Reprojection error	0.43 pix (1.76 max)	0.40 pix (3.75 max)	0.38 pix (1.20 max)
GCPs error	1.52 m 1.48 pix	1.14 m 1.96 pix	0.62 m 1.86 pix
Image quality	Ultra high	High	High
Mean GSD	0.16 m/pix	0.22 m/pix	0.064 m/pix
Dense point cloud	49,844,094 pts	55,114,074 pts	56,171,705 pts
Point density	37 pts m^{-2}	20 pts m^{-2}	244 pts m^{-2}
Post-processing data			
Filtered point cloud /subsampled	15,617,342 pts (sampled 0.20 m)	24,226,221 pts (sampled 0.20 m)	4,517,143 pts (sampled 0.10 m)
Point density	8 pts m^{-2}	9 pts m^{-2}	21 pts m^{-2}
ICP transformation	0.14 m	0.15 m	0.10 m

950

951

952

953

Table 3. Results of comparisons between SfM-MVS-based DEMs vs. ALS-based DEMs in the common area and for the bare-ground stable area and glacier.

DEMs	Elevation differences [m] cell size 1 m x 1m							
	Common SfM-MVS bare-ground area				Common SfM-MVS glacier area			
	Min	*Max*	*Mean*	*σ*	*Min*	*Max*	*Mean*	*σ*
SfM-MVS 2013 - ALS 2013	-19.59	33.61	-0.42	1.72	-9.91	12.04	-0.13	0.78
SfM-MVS 2014 - ALS 2014	-18.48	22.42	0.03	0.74	-18.17	11.41	0.23	0.65
SfM-MVS 2014 - SfM-MVS 2013	-33.12	14.19	0.38	1.73	-12.44	12.33	1.58	1.42
ALS 2014 - ALS 2013	-15.38	10.81	-0.09	0.29	-14.61	7.37	1.30	0.97

Table 4. Mass balance calculations on La Mare Glaciers using different combinations of SfM-MVS and ALS DEMs.

DEMs cell size 10 m	Mass balance estimation						
	Spatial coverage [m^2]	Average elevation changes [m]		Volume change [m^3]		Mass balance [m w.e]	
		Raw	*Corrected*	*Raw*	*Corrected*	*Raw*	*Corrected*
SfM-MVS 2014 - SfM-MVS 2013	1,834,800 (~88%)	1.81	1.45	3,320,988	2,660,460	1.09	0.87
ALS 2014 - ALS 2013		1.47	1.56	2,697,156	2,862,288	0.88	0.94
SfM-MVS 2014 - ALS 2013	1,938,700 (~93%)	1.64	1.70	3,179,468	3,295,790	0.98	1.02
ALS 2014 - ALS 2013		1.41	1.50	2,733,567	2,908,050	0.85	0.90
ALS 2014 - ALS 2013	2,072,700 (entire glacier)	1.43	1.52	2,963,961	3,150,504	0.86	0.91

Table 5. Statistics of elevation changes in the rock glacier and in ~~bed~~ bare ground stable area off rock glacier from September 2014 to September 2013 and September 2003 in the ALS reconstructed area and in the common ALS and SfM-MVS coverage area.

Elevation changes [m]									
Data			ALS Reconstructed area				SfM-MVS Reconstructed area			
			Stable area		Rock glacier		Stable area		Rock glacier	
			Mean	*σ*	*Mean*	*σ*	*Mean*	*σ*	*Mean*	*σ*
SfM 2014	-	ALS 2014	—	—	—	—	0.05	0.31	0.02	0.17
SfM 2014	-	ALS 2013	—	—	—	—	0.01	0.33	-0.04	0.18
ALS 2014	-	ALS 2013	-0.05	0.19	-0.07	0.12	-0.05	0.20	-0.07	0.12
SfM 2014	-	ALS 2003	—	—	—	—	0.06	0.33	-0.16	0.49
ALS 2014	-	ALS 2003	-0.01	0.22	-0.18	0.46	-0.00	0.21	-0.18	0.47
ALS 2013	-	ALS 2003	0.04	0.21	-0.11	0.41	—	—	—	—

Table 6. Velocity statistics in three distinct areas of the rock glacier and in stable area outside the rock glacier evaluated comparing the 2003 and 2014 ALS DEMs and the photogrammetric DEM for the 2014 survey epoch.

Horizontal movements between 2003 and 2014 [cm yr $^{-1}$]										
	ALS 2003 - ALS 2014					ALS 2003 - SfM-MVS 2014				
	No. points	*Min*	*Max*	*Mean*	*σ*	*No. points*	*Min*	*Max*	*Mean*	*σ*
Area 1	41	7.3	43.3	26.8	8.9	36	6.8	47.5	26.3	10.3
Area 2	13	4.4	27.4	18.9	7.0	11	9.0	27.9	18.1	6.4
Area 3	26	4.5	16.5	9.4	4.0	24	4.5	18.2	9.0	4.1
Off rock glacier	65	0.0	10.7	3.6	3.1	23	0.0	13.6	5.3	4.2

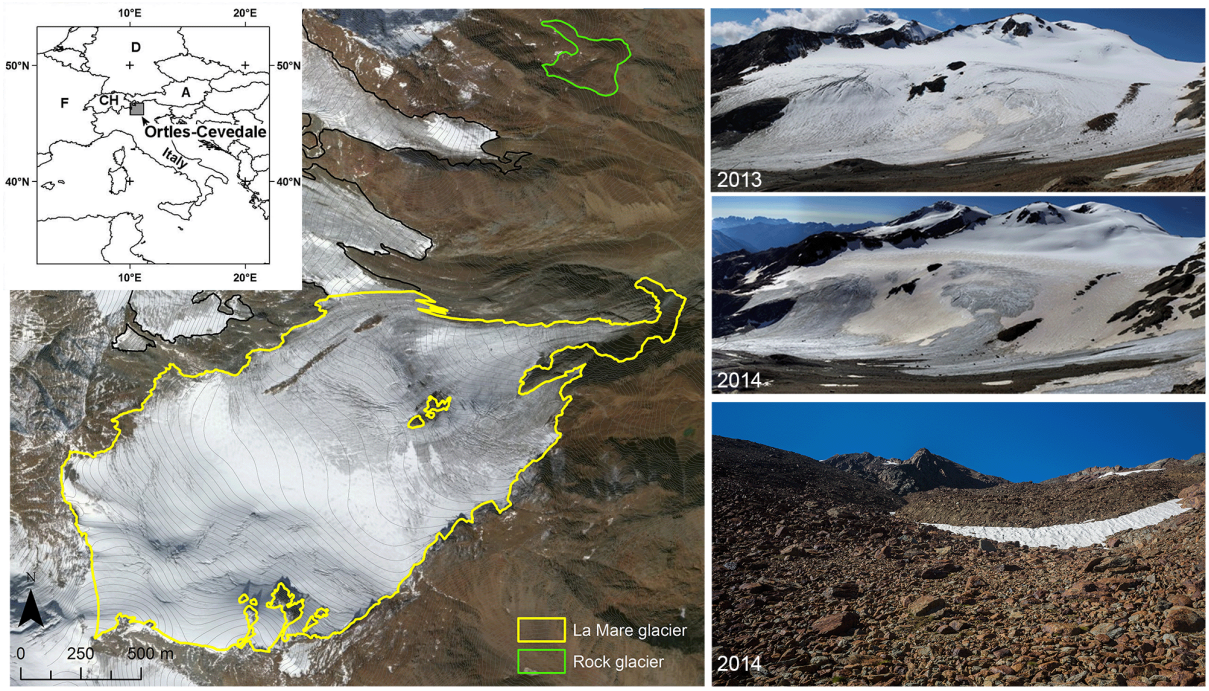

Figure 1. Geographic setting of study areas. Panorama view of the La Mare Glacier from the same camera position on 4 September 2013 and 27 September 2014. The lower right photograph shows the front of the meridional lobe of the AVDM3 Rock Glacier, which was surveyed on 27 September 2014.

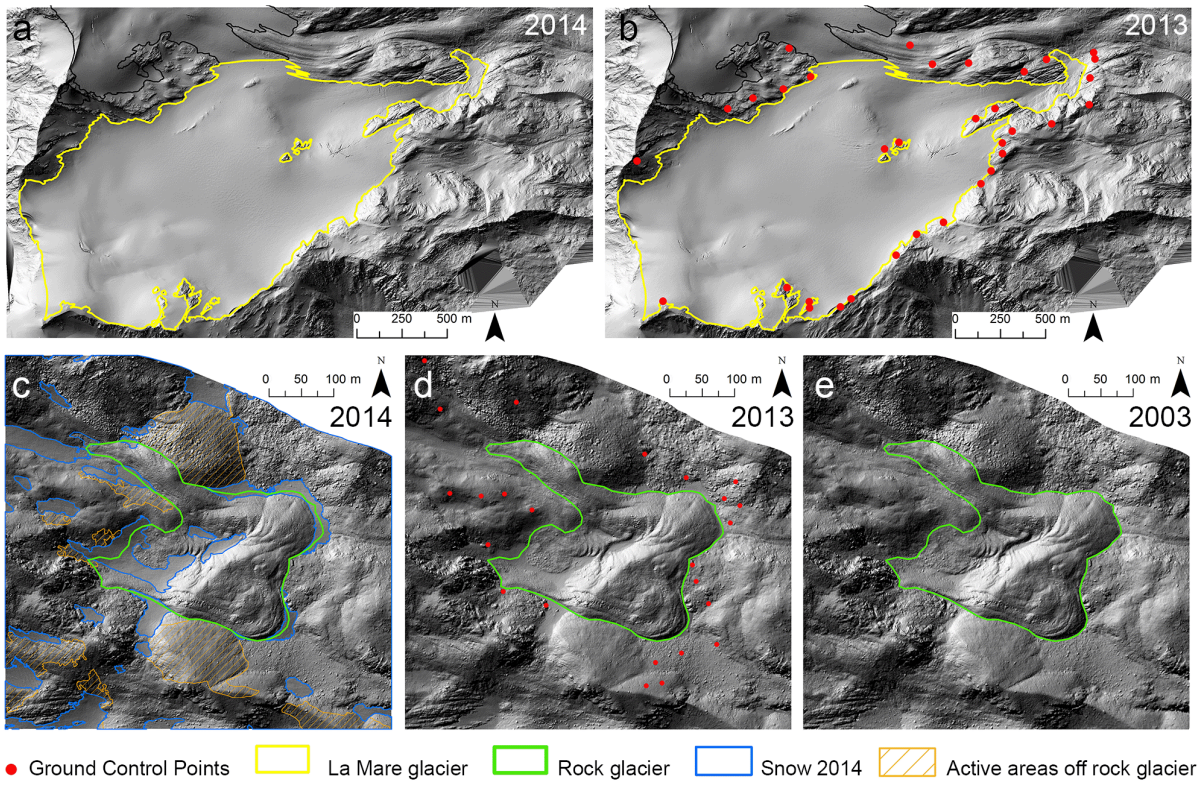

Figure 2. ALS shade DEMs of la Mare glacier acquired on **(a)** September 24, 2014 and **(b)** September 21, 2013. The ALS DEMs of rock glacier acquired on **(c)** 2014, **(d)** 2013 and **(e)** 2003.The red dots represent the selected GCPs in 2013 DEM used in the photogrammetric approach. The snow accumulation areas and geomorphologically-active areas outside the rock glacier were excluded during the ICP computation between 2013 and 2003, 2014 ALS point cloud.

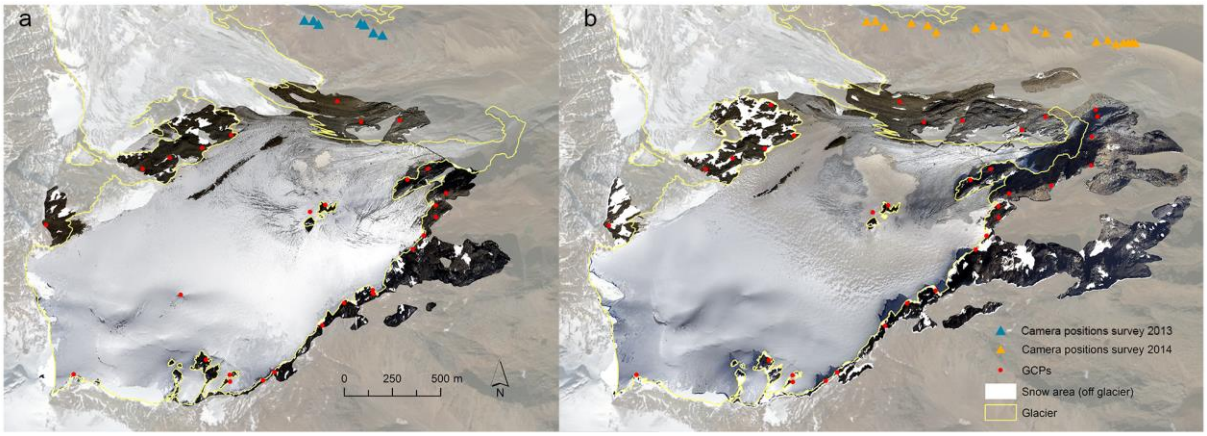

Figure 3. Orthophoto-images of SfM-MVS 3D model of La Mare glacier surveyed on **(a)** 4 September 2013 and **(b)** 27 September 2014. The white areas in the ortho-images represent the snow-covered area in the rock stable area. The red dots outside the glacier area are the GCPs and the triangles identified the camera locations.

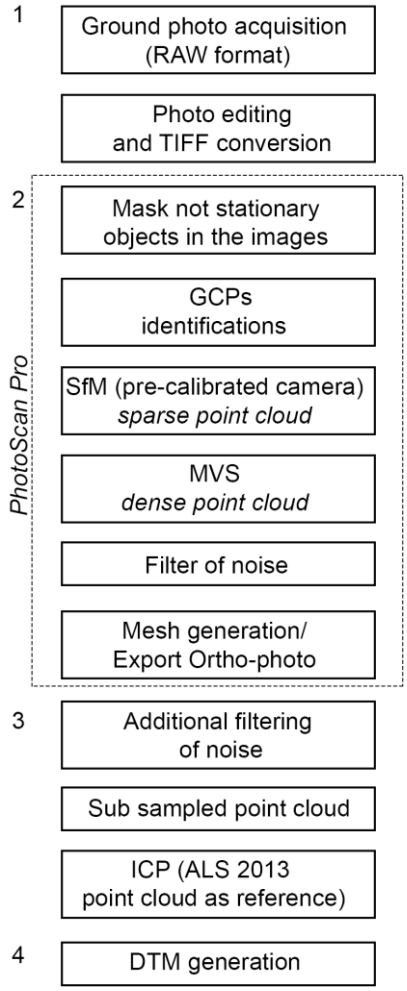

Figure 4. Workflow illustrating the photo-based 3D reconstruction process used in this work for both case studies, starting from images collection to DEM generation.

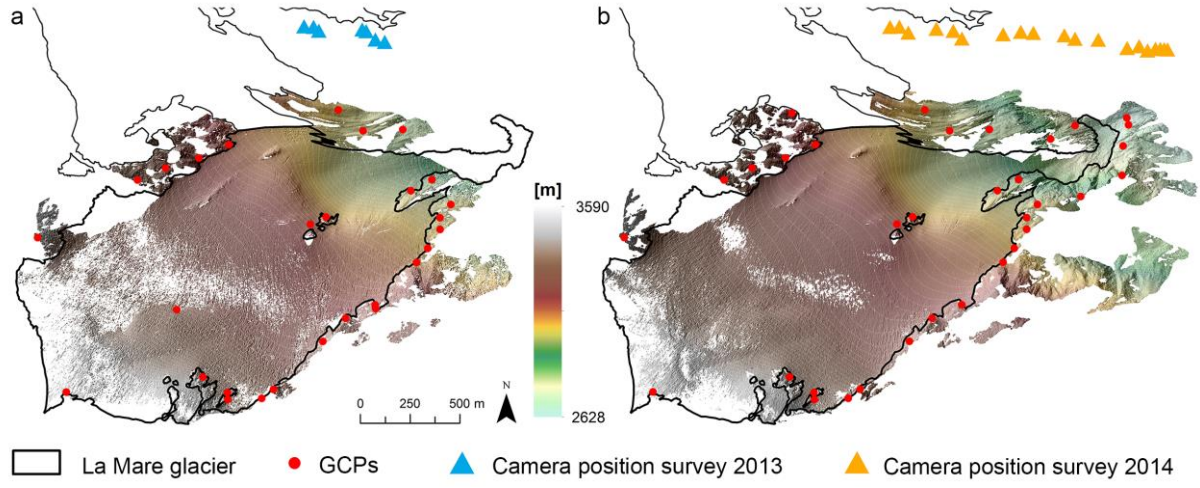

Figure 5. Hillshaded DEMs of La Mare glacier derived from photogrammetric measurements on **(a)** 4 September 2013 and **(b)** 27 September 2014.

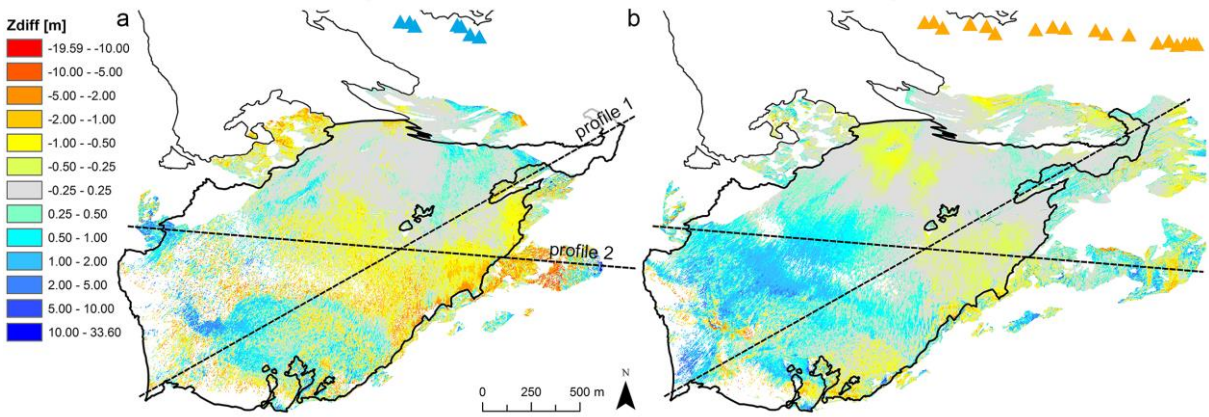

Figure 6. Spatial distribution of elevation differences between photogrammetric and ALS-based DEMs on **(a)** 2013 and **(b)** 2014.

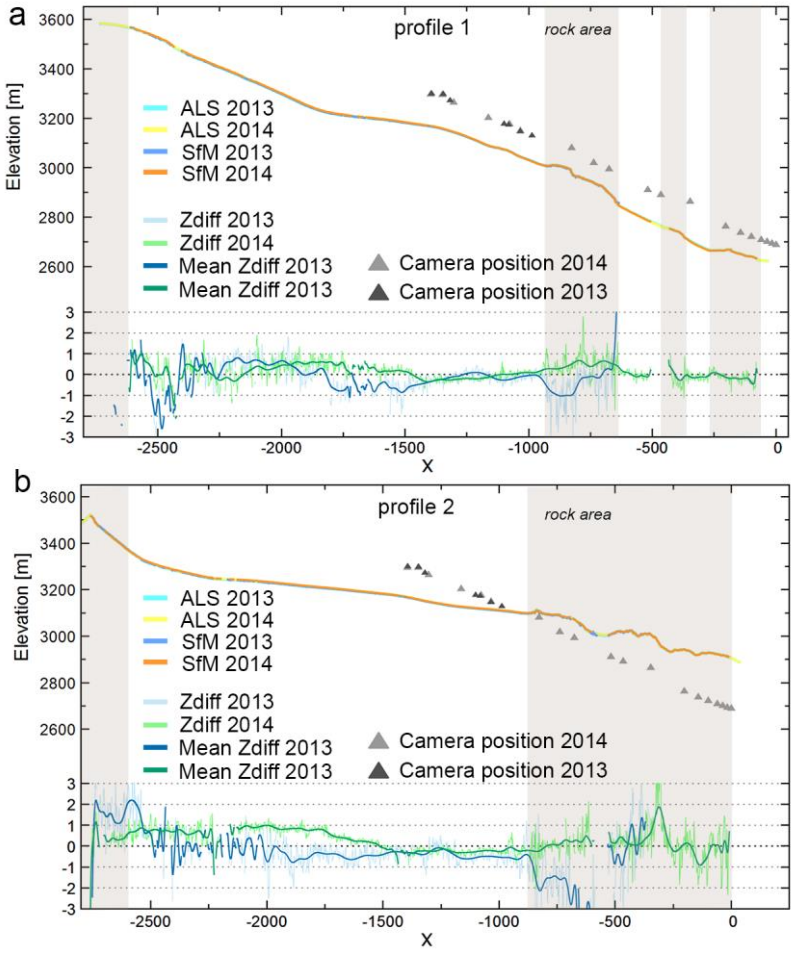

Figure 7. Cross sections through the La Mare glacier DEMs show the glacier elevation change and the difference between 2013 and 2014 in SfM-MVS and ALS-based DEMs. The location of **(a)** the profile 1 and **(b)** profile 2 is indicated in Fig. 6. The x-axis zero has been fixed at the first camera position of the 2014 survey and the minimum and maximum values of the z-difference set to ± 3 m.

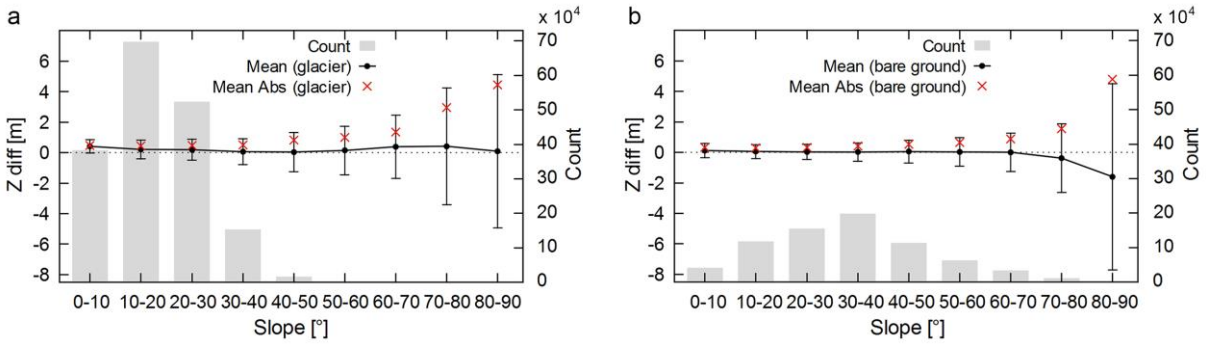

Figure 8. Mean, mean of the absolute values and standard deviation of the 2014 DoD between SfM-MVS and ALS-based DEM depending on slope calculated **(a)** in

the glacier area and **(b)** in the bare ground outside glacier covered by rock. The grey bars show the count of cells at any given slope (y-axis on the right).

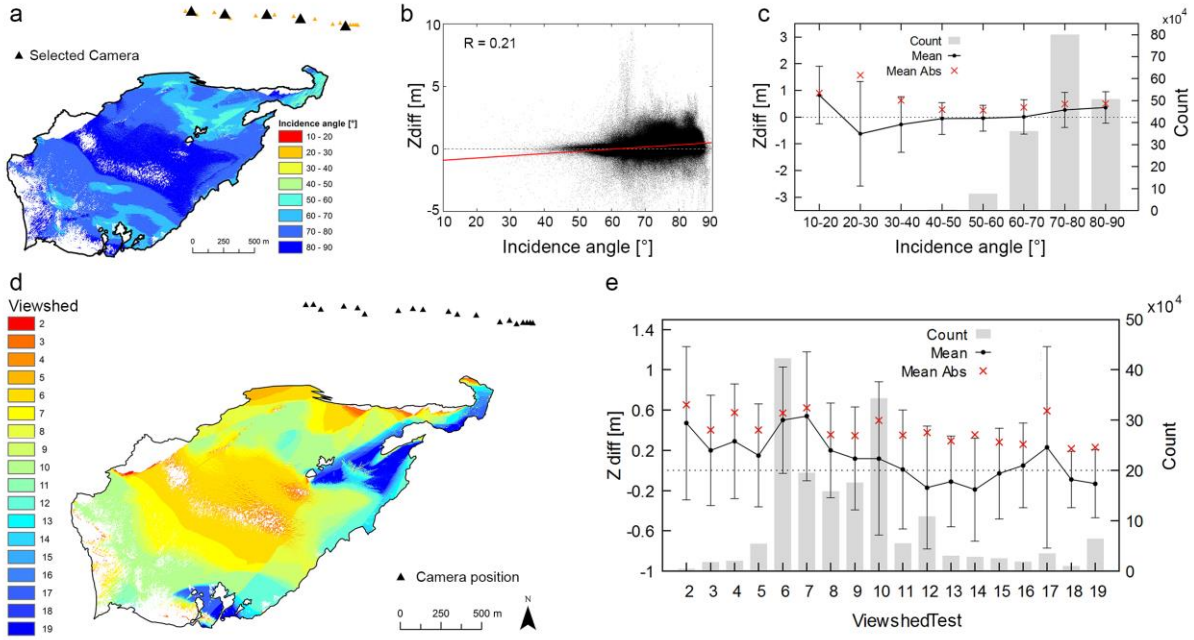

Figure 9. Mean incidence angles between five cameras positions and vectors normal to the surface and viewshed analysis. **(a)** Map of the mean incidence angle calculated for five representative camera positions; **(b)** the scatterplot of the elevation difference and the mean incidence angle for the five camera positions; **(c)** mean with one standard deviation y bars and mean of the absolute value of elevation differences for the mean incidence angle intervals calculated for 5 selected camera; **(d)** map of the viewshed reconstructed area visible from all camera; **(e)** mean with one standard deviation y bars and mean of the absolute value of elevation differences for the viewshed reconstructed area.~~Mean iIncidence angles between five cameras positions and vectors normal to the surface. **(a)** Map of the mean incidence angle calculated for five representative camera positions; **(b)** the scatterplot of the elevation difference and the mean incidence angle for the five camera positions; **(c)** mean with one standard deviation y bars and mean of the absolute value of elevation differences for the mean incidence angle intervals calculated for 5 selected camera; **(d)** map of the viewshed reconstructed area visible from all camera; **(e)** mean with one standard deviation y bars and mean of the absolute value of elevation differences for the viewshed reconstructed area.~~

~~Frequency distribution histograms of incidence angles calculated for the corresponding surface and **(b)** the scatterplot of the elevation difference and incidence angle for the five camera positions; **(c)** mean of elevation differences with one standard deviation y bars calculated for each camera and for incidence angle intervals; **(d)** map of the locations of the selected cameras with the viewshed reconstructed area visible from each camera point.~~

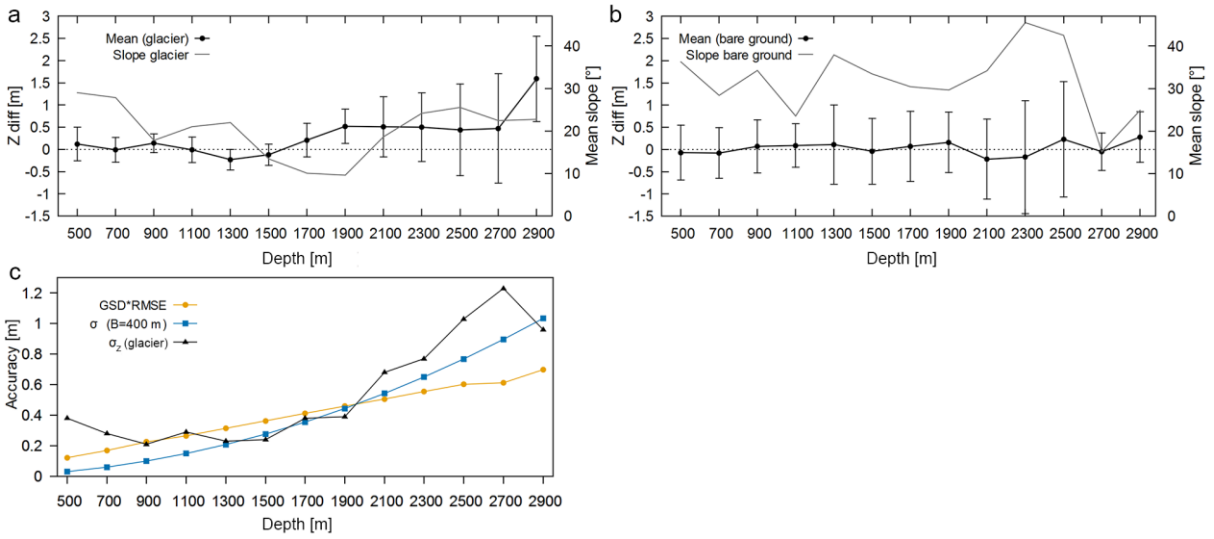

Figure 10. Mean and standard deviation of the 2014 DoD between SfM-MVS and ALS-based DEM depending on depth calculated **(a)** in the glacier area and **(b)** in the bare ground outside glacier covered by rock. The trend of the average slope angle for depth intervals is shown on the right y-axis. **(c)** Comparison of σ_z measured in the glacier reconstructed area, the theoretical depth accuracy estimated according to the Eq. (1) and the GSD multiplied for the GCPs RMSE for the depth intervals.

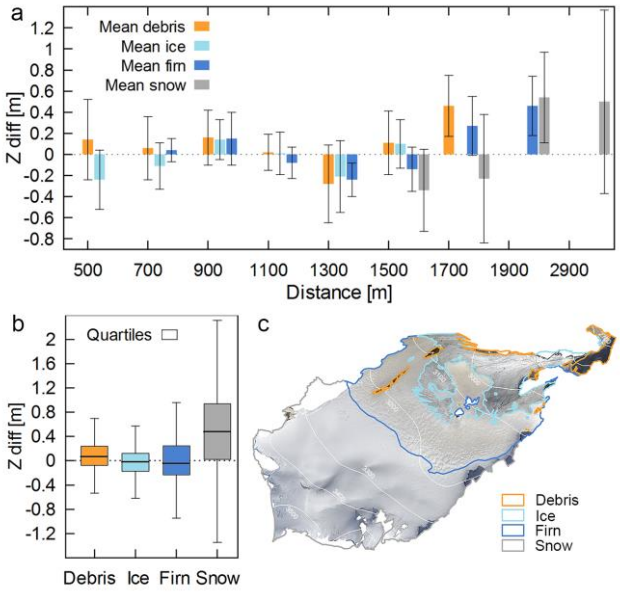

1065

1066 **Figure 11**. Elevation difference between the 2014 SfM-MVS and ALS-based DEMs
1067 calculated for different substrata. The figure shows **(a)** the mean and standard
1068 deviation of z-difference for four substrata (debris, ice, firn, and snow) grouped by
1069 distance from camera position; **(b)** the box plot of the z-difference for four substrata.
1070 In the box-whisker plot, values which exceed 1.5 * IQR were considered outliers. In
1071 panel **(c)** the orthophoto of the glacier on 27 September 2014 and map of substrata.

1072

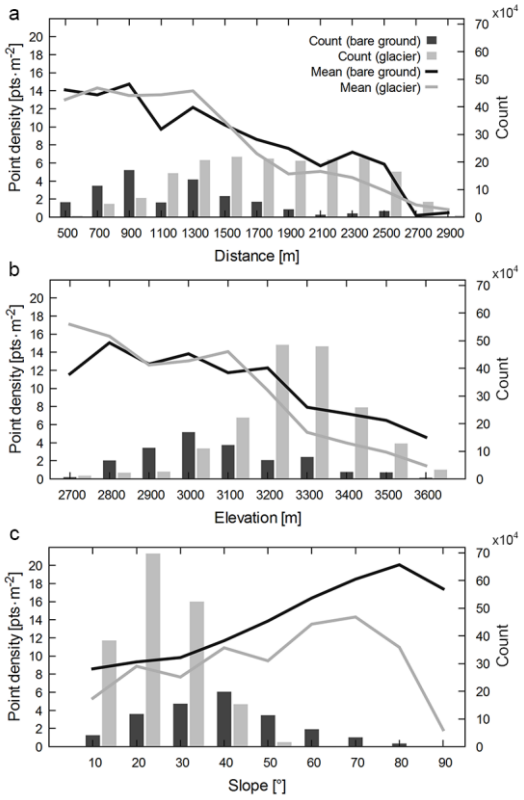

1073

1074 **Figure 12**. Relationships between point density of the 2014 photogrammetric 3D
1075 model and **(a)** camera-object distance, **(b)** elevation and **(c)** slope calculated for the
1076 glacier and rock stable area outside glacier. The point density was estimated using
1077 the filtered and subsampled point cloud.

1078

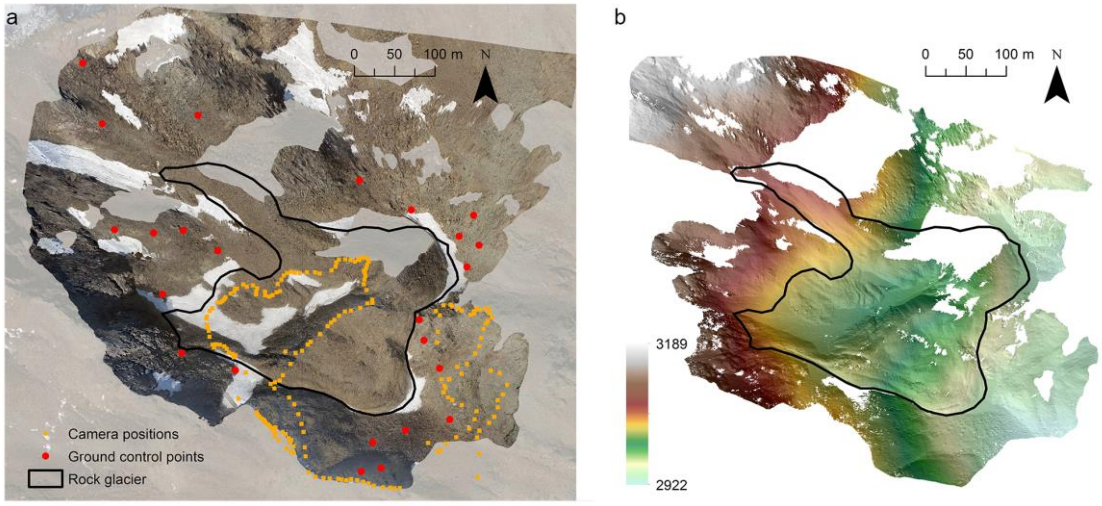

1079

1080 **Figure 13**. Correspondence between **(a)** the orthophoto of SfM-MVS 3D model of
1081 rock glacier surveyed on 27 September 2014 and **(b)** the hillshade model of rock

glacier model calculated at the same data and hour of the images acquisition. The holes in the DEM represent not reconstructed area.

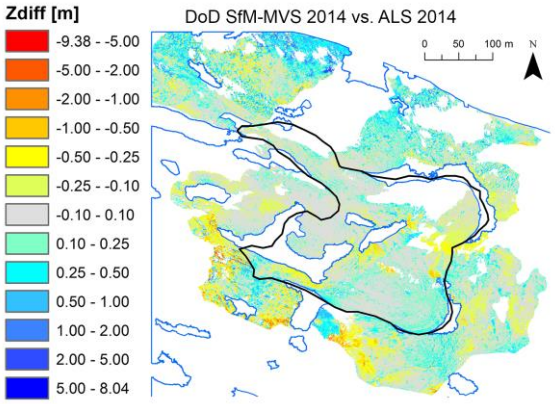

Figure 14. Spatial distribution of elevation differences between photogrammetric and ALS-based DEM acquired on 27 September 2014 and 24 September 2014, respectively. The blue shape is the snow accumulation areas excluded during the DEMs comparison.

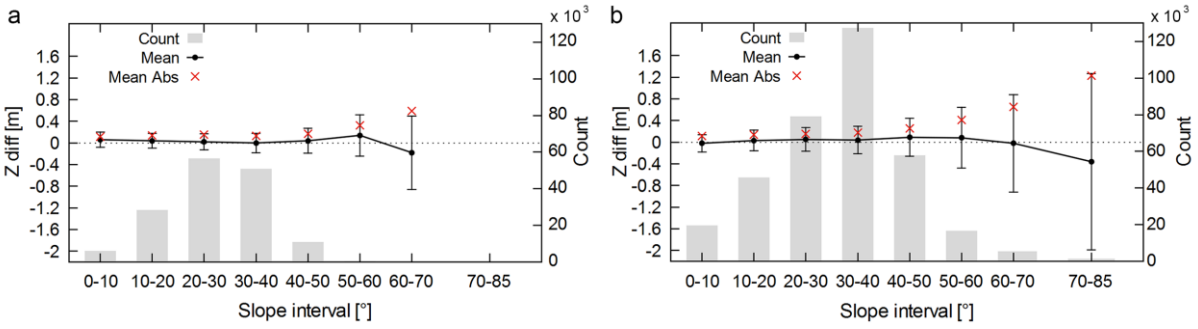

Figure 15. Mean, mean of the absolute values and standard deviation of elevation differences between 2014 SfM-MVS and ALS-based DEMs calculated for the slope interval **(a)** in the rock glacier reconstructed area and **(b)** in the bare ground outside the rock glacier.

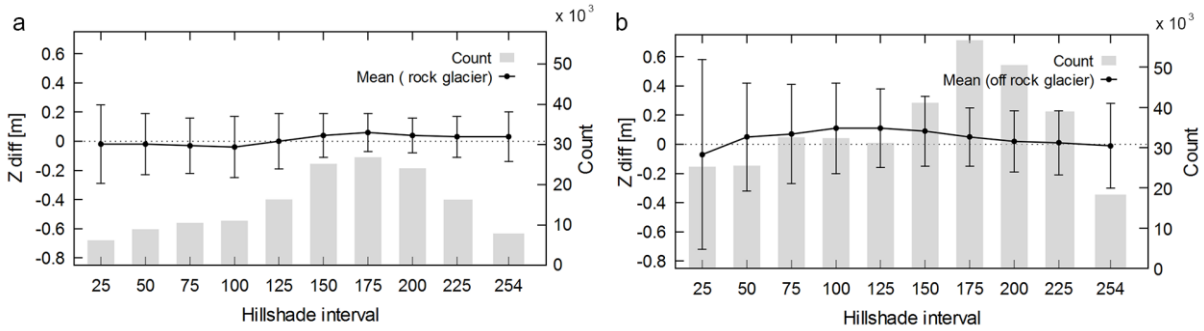

1097

1098 **Figure 16**. Elevation differences between 2014 SfM-MVS and ALS-based DEMs
1099 calculated for the hillshade interval **(a)** in the rock glacier reconstructed area and **(b)**
1100 in the bare ground outside the rock glacier. Lowest values represent shadowed area
1101 whilst lighted areas present the highest values.

1102

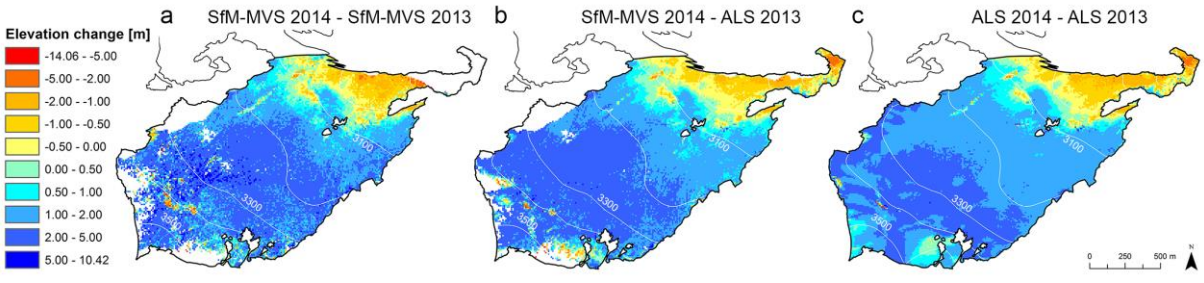

1103

1104 **Figure 17**. Spatial distribution of elevation changes between **(a)** SfM-MVS 2014 and
1105 SfM-MVS 2013 DEMs **(b)** SfM-MVS 2014 and ALS 2013 over the area of the glacier
1106 with common coverage and **(c)** ALS 2014 and ALS 2013 over the entire glacier.

1107

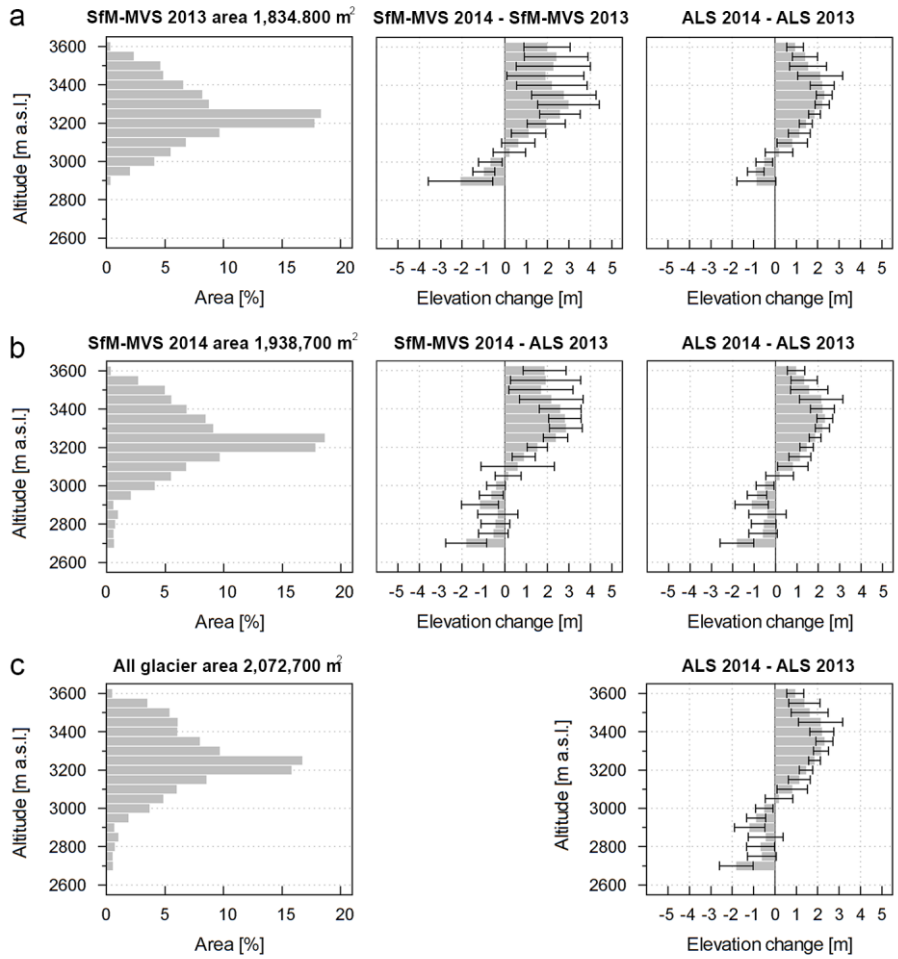

Figure 18. Area-altitude distribution and surface elevation change with standard deviation for the glaciological year 2014/2013 displayed for altitudinal bands with 50 m interval. The elevation change were calculated between **(a)** SfM-MVS DEMs of 2013 and 2014 in the 2013 photogrammetric reconstructed area; **(b)** SfM-MVS DEMs of2014 and ALS DEM of 2014 in the 2014 photogrammetric reconstructed area; **(c)** ALS DEMs of 2013 and 2014 of the entire glacier. The photogrammetric results were compared with the corresponding ALS result calculated in the same area.

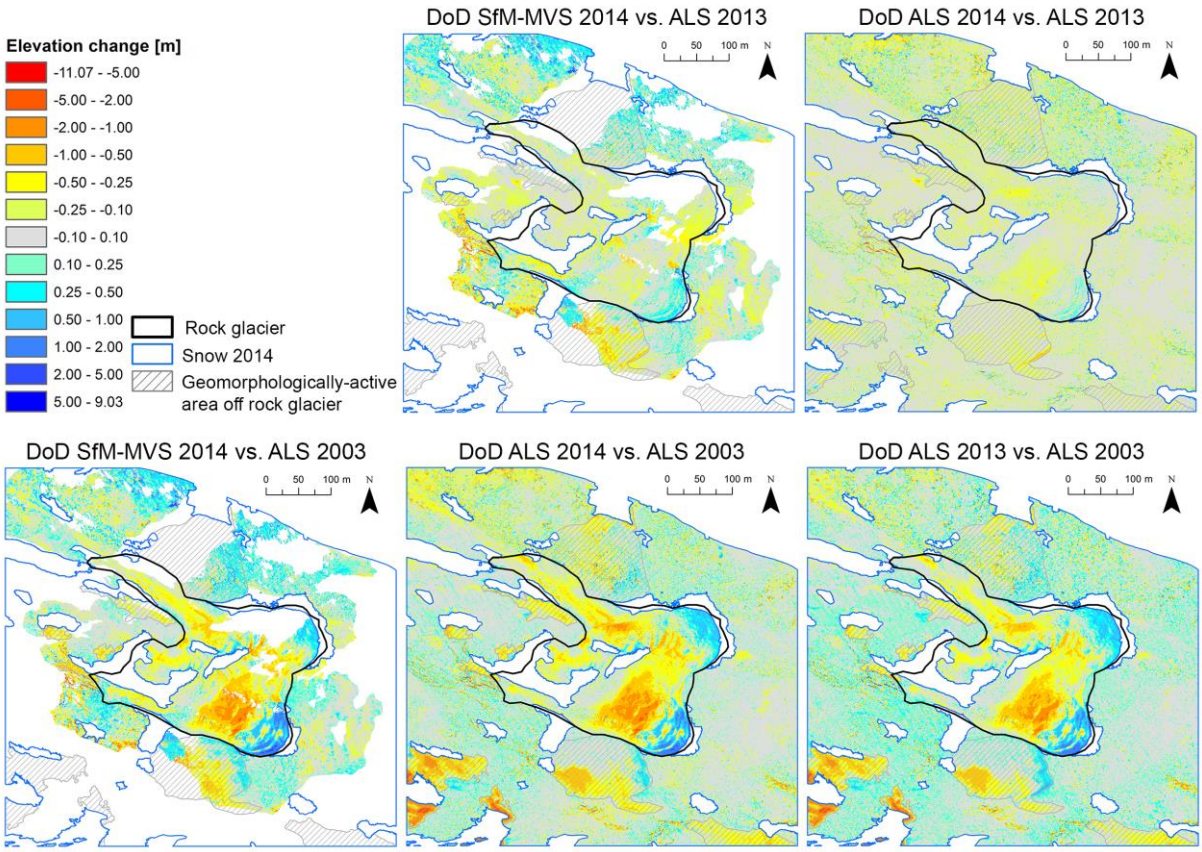

1117

1118 **Figure 19**. Spatial distribution of elevation changes from September 2014 to
1119 September 2013 and September 2003 between the DEMs derived from SfM-MVS
1120 and ALS.

1121

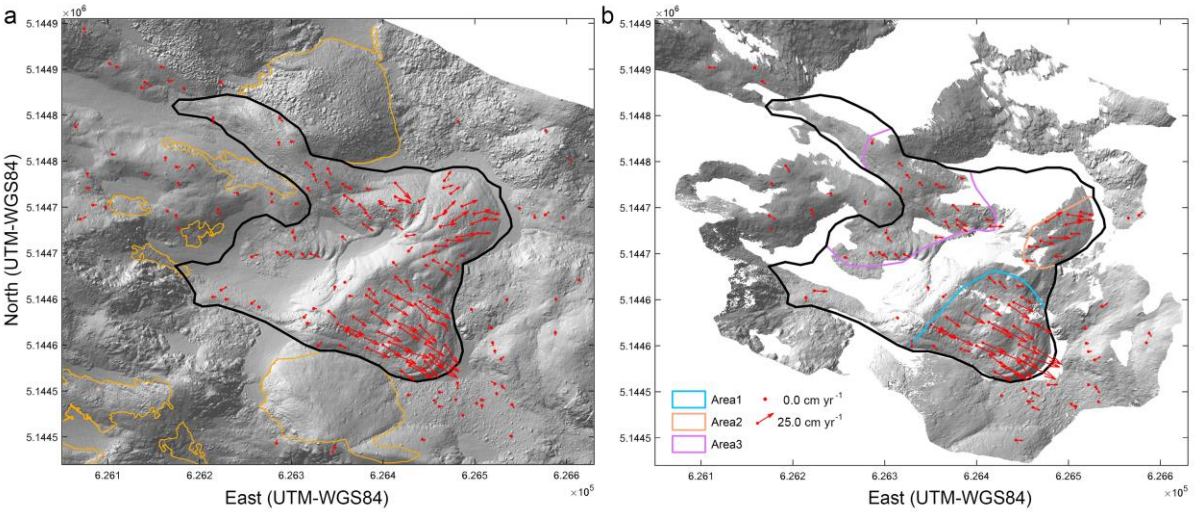

1122

1123 **Figure 20**. Displacement vectors of the rock glacier between 2003 and 2014
1124 computed by a manual identification of natural features visible in the shaded DEMs

generated by **(a)** ALS for both survey epochs and by **(b)** ALS and photogrammetry for 2003 and 2014 survey, respectively.